Boron and Lithium in Calcium Sulfate Veins: Tracking Precipitation of Diagenetic Materials in Vera Rubin Ridge, Gale Crater

D. Das, P. Gasda, R. Wiens, K. Berlo, R. Leveille, J. Frydenvang, N. Mangold, R. Kronyak, S. P Schwenzer, O. Forni, et al.

Boron and Lithium in Calcium Sulfate Veins: Tracking Precipitation of Diagenetic Materials in Vera Rubin Ridge, Gale Crater

Das Debarati (Orcid ID: 0000-0001-9453-799X)
Gasda Patrick, J (Orcid ID: 0000-0003-0895-1153)
Wiens Roger, C. (Orcid ID: 0000-0002-3409-7344)
Frydenvang Jens (Orcid ID: 0000-0001-9294-1227)
Mangold Nicolas (Orcid ID: 0000-0002-0022-0631)
Kronyak Rachel, Emily (Orcid ID: 0000-0002-2740-5660)
Schwenzer Susanne, P (Orcid ID: 0000-0002-9608-0759)
Forni Olivier (Orcid ID: 0000-0001-6772-9689)
Cousin Agnès (Orcid ID: 0000-0001-7823-7794)
Gasnault Olivier (Orcid ID: 0000-0002-6979-9012)

Boron and Lithium in Calcium Sulfate Veins: Tracking Precipitation of Diagenetic Materials in Vera Rubin Ridge, Gale Crater

D. Das[1], P. J. Gasda[2], R. C. Wiens[2], K. Berlo[1], R. J. Leveille[1], J. Frydenvang[3], N. Mangold[4], R. E. Kronyak[5], S. P. Schwenzer[6], Olivier Forni[7], Agnes Cousin[7], S. Maurice[7], O. Gasnault[7]

[1]Department of Earth and Planetary Sciences, McGill University, Quebec, Canada H3A 0E8.
[2]Los Alamos National Laboratory, Los Alamos, NM, USA 87545.
[3]University of Copenhagen, Copenhagen, Denmark.
[4]Laboratoire de Planétologie et Géodynamique, UMR6112 CNRS, Université de Nantes, Université Angers, Nantes, France.
[5]Department of Earth and Planetary Sciences, University of Tennessee, Knoxville, TN USA.
[6]AstrobiologyOU, School of Environment, Earth and Ecosystem Sciences, The Open University, Milton Keynes, United Kingdom
[7]Institut de Recherche en Astrophysique et Planetologie, Universite de Toulouse, CNRS, CNES, Toulouse, France.

Corresponding author: Debarati Das (debarati.das@mail.mcgill.ca)

This article has been accepted for publication and undergone full peer review but has not been through the copyediting, typesetting, pagination and proofreading process which may lead to differences between this version and the Version of Record. Please cite this article as doi: 10.1029/2019JE006301

Key Points:

- ChemCam analyses of calcium sulfate veins in Vera Rubin ridge (VRR) show the presence of boron and lithium.
- Boron detection frequency in the Ca-sulfate veins increases in the Jura member of VRR and is inversely correlated with lithium.
- The relationship between B and Li suggests an evaporative sequence formed during dehydration on higher elevations of VRR.

Abstract

The NASA *Curiosity* rover's ChemCam instrument suite has detected boron in calcium-sulfate-filled fractures throughout the sedimentary strata of Gale crater including Vera Rubin ridge (VRR). The presence of elevated B concentration provides insights into Martian subsurface aqueous processes. In this study we extend the dataset of B in Ca-sulfate veins across Gale crater, comparing the detection frequency and relative abundances with Li. We report 33 new detections of B within veins analyzed between sols 1548 and 2311 where detections increase in Pettegrove Point and Jura members, which form VRR. The presence of B and Li in the Ca-sulfate veins is possibly due to dissolution of pre-existing B in clays of the bedrock by acids or neutral water and redistribution of the elements into the veins. Elevated frequency of B detection in veins of Gale crater correlate with presence of dehydration features such as desiccation cracks, altered clay minerals and detections of evaporites such as Mg-sulfates, chloride salts in the host rocks. The increased observations of B also coincide with decreased Li concentration in the veins (average Li concentration of veins drops by ~15 ppm). Boron and Li have varying solubilities and Li does not form salts as readily upon dehydration as B, causing it to remain in the solution. So, the weak negative correlation between B and Li may reflect the crystallization sequence during dehydration on Vera Rubin ridge.

Plain Language Summary

Boron and lithium were measured in cracks in the rocks that were filled with whitish, calcium sulfate. These were found in Gale crater using the ChemCam instrument on the Mars Science Laboratory *Curiosity* rover. Both elements are highly water-soluble and may indicate late-stage ground water activity. Boron's lower solubility compared to that of lithium means it forms salts relatively easily while Li remains dissolved in the brine with progressive evaporation. In our study we find that on Vera Rubin ridge, boron detection frequency is inversely proportional to the concentration of lithium. This finding suggests that, based on their different solubilities, boron precipitated in the fractures before lithium. Lithium possibly moved away downhill with the remaining brine, leaving boron behind as precipitates.

1 Introduction

Boron is a light, soluble element that is found on Earth as borates in evaporite deposits and in clay-bearing sediments. The high solubility of B (as $B(OH)_3$ in acid and $B(OH)_4^-$ in alkaline water) makes it a good tool for understanding surface and sub-surface aqueous processes (Hunt, 1966; Lerman, 1966; Couch and Grim, 1968; Tanner, 2002; Helvaci and Ortí, 2004; Grew, 2017; Helvaci and Palmer, 2017). Characterization of borate phases enables the reconstruction of fluid temperature, salinity, and pH conditions in sedimentary systems (Frederickson and Reynolds, 1960; Lerman, 1966; Harder, 1970; Perry, 1972; Keren and Mezuman, 1981; Miranda-gasca *et al.*, 1998; Helvaci and Ortí, 2004).

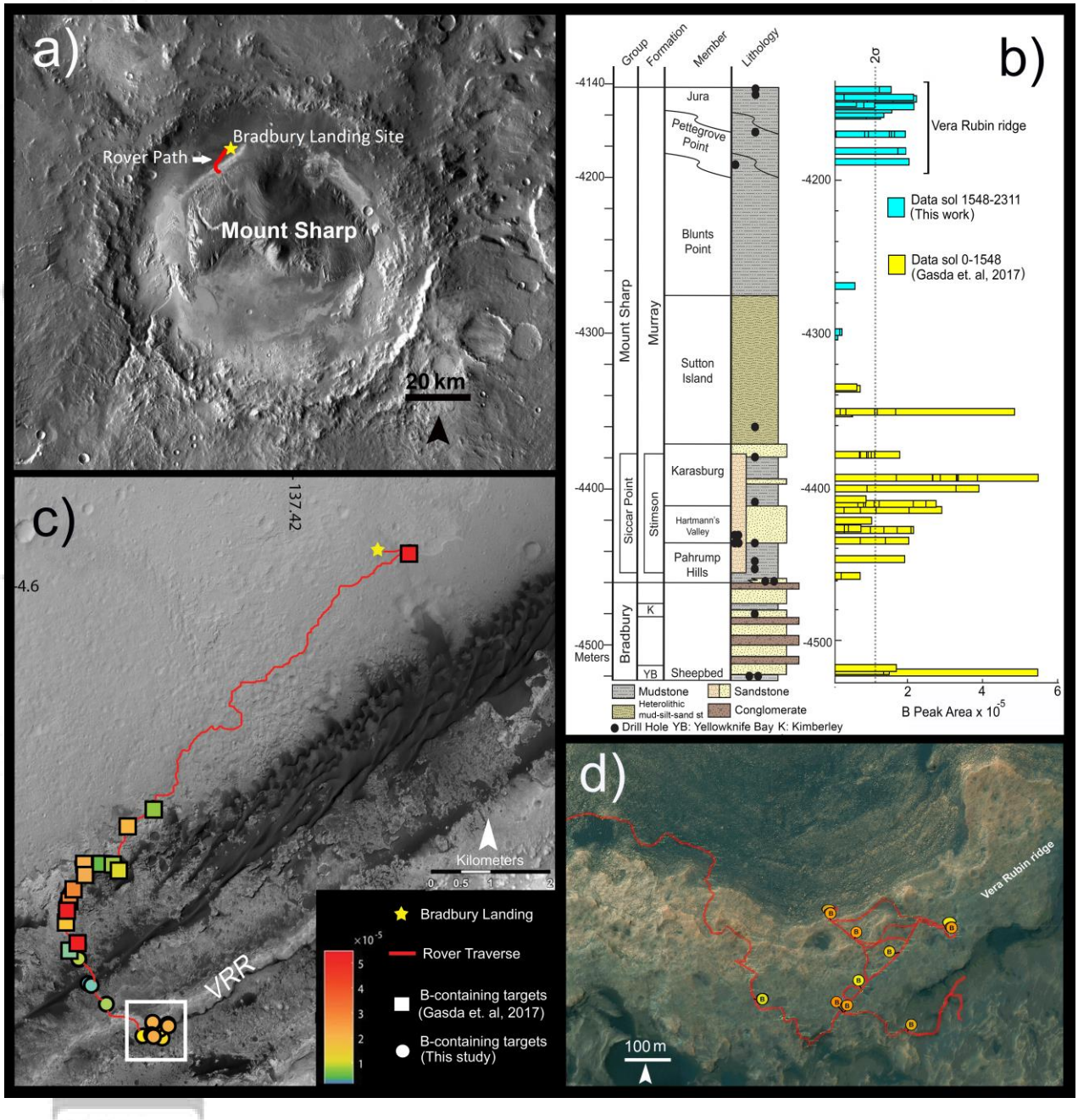

Figure 1. Overview of Curiosity's Gale Crater sampling area and summary of boron detections in the Vera Rubin ridge area. **a)** Gale Crater with red line indicating Curiosity's traverse from Bradbury Landing site to the rover position on Sol 2052. **b)** Gale Crater stratigraphic column with normalized peak area for each boron detection plotted as bars versus elevation. **c)** The rover traverse map showing boron detection locations. Colors on the filled squares and circles represent the normalized boron peak area according to the color bar. **d)** MRO HiRISE image of Vera Rubin ridge indicating the boron detection locations with the same color scheme as shown in Figure 1C.

Borates can stabilize ribose, the simple sugar that forms the backbone of ribonucleic acid (RNA) (Kim *et al.*, 2011; Furukawa *et al*., 2013; Furukawa and Kakegawa, 2017). Without borate ions, ribose decomposes in water within a geologically short time (ribose half-life is 300 days at 25°C and pH 7.0) (Larralde *et al*., 1995). Although there are numerous hypotheses proposed for the origin of life (Ruiz-mirazo *et al.*, 2013), the most recent work on prebiotic chemical syntheses of RNA nucleotides proposes wet-dry cycles in the presence of salts like borates, nitrites, and carbonates, where boric acid is a reagent that assists in the reaction (Powner *et al*., 2009; Becker *et al.*, 2016, 2019; Hud and Fialho, 2019). The NASA *Curiosity* rover detected B in 43 locations along its traverse in Gale crater (Gasda *et al*., 2017). These observations, along with the recent discovery of organic molecules on Mars (Ming *et al.*, 2014; Eigenbrode *et al.*, 2018) and ribose in chondrites (Furukawa *et al.*, 2019) provide a basis for the possibility of prebiotic chemical reactions involving borates having occurred on Mars.

The Mars boron observations were made using the ChemCam instrument suite while targeting Ca-sulfate filled fractures or "veins". Boron has been primarily detected in veins hosted in phyllosilicate-rich lacustrine Yellowknife Bay and Murray formation mudstones. The B enrichment likely occurred during a sequence of events that include initial deposition of B in evaporite layers in stratigraphically higher units, followed by later groundwater dissolution of the evaporites, transportation to underlying layers, and co-precipitation of borates in fractures along with Ca-sulfate (Gasda *et al.*, 2017). Concentrations of 154–166 ppm B have also been detected in clays within Martian meteorites (Stephenson *et al.*, 2013). While remote detection of borates is possible (e.g, Cloutis *et al*., 2016), the authors are not aware of borate detections made by orbital remote sensing instruments or by other in situ Curiosity instruments such as CheMin. Evaporite elements including Cl, Na, and, S are detected on Mars using ground-based observations (Baird *et al*., 1976) (evaporite minerals including sulfates and chlorides detected from orbit :e.g., Glotch *et al.*, 2010; Ehlmann *et al.*, 2016), co-enrichments of Na and Cl observed with ground-based observations (Thomas *et al*., 2018, 2019; Rapin *et al*., 2019) and evaporite minerals including gypsum, anhydrite, basanite, and chloride salts detected by CheMin (Vaniman *et al*., 2018; Morris *et al.*, 2019; Thomas *et al.*, 2018, 2019). Based on the detection of these evaporites, we infer the possible presence of borate evaporites on Mars.

2 Geologic context

Gale crater is a ~155 km diameter impact crater with a central mound (Aeolis Mons, informally known as "Mt. Sharp") (Figure 1A), located in the northwestern part of the Aeolis quadrangle (Grotzinger and Milliken, 2012).

In 2012, NASA's Mars Science Laboratory (MSL) *Curiosity* rover landed on Aeolis Palus. The rover has traversed ~22 km from the Bradbury Rise landing site, across outcrops of fluvio-lacustrine deposits (Grotzinger *et al.*, 2014, 2015; Vasavada *et al*., 2014) and local eolian deposits (Banham *et al.*, 2018). The geology of Gale crater points to an ancient environment with a long duration water body that would have been habitable (Grotzinger *et al.*, 2015). A stratigraphic column depicting the sedimentary facies encountered is shown in Figure 1B. The first facies, belonging to the Bradbury group, is a fluvio-deltaic deposit exposed along the crater floor, interfingered with the Mount Sharp group (Grotzinger *et al.*, 2015). The deposits of this group include mudstones, sandstones, and conglomerates; low levels of chemical weathering suggesting a relatively cold climate and minimal water-rock interaction (McLennan *et al.*, 2014). The Mount Sharp group consists of the Murray formation, which is largely lacustrine in origin and shows more significant indications of chemical weathering (Mangold *et al.*, 2019). The Mount Sharp group also present features that are interpreted as lake margin and evaporitic environments (Kah *et al.*, 2018; Stein *et al.*, 2018; Rapin *et al.*, 2019). The Siccar Point group unconformably overlies the Murray formation of the Mount Sharp Group, and is interpreted as a younger deposit of basaltic eolian sandstone (Banham *et al*., 2018; Siebach *et al.*, 2019).

2.1 Mount Sharp Group—Murray Formation

The Murray formation (Figure 1B) is currently divided into seven members (Fedo *et al.*, 2018; Siebach *et al*., 2019), representing a series of lake deposits that experienced episodic drying. New members could be defined as the rover continues to move up-section from VRR. The Pahrump Hills member is interpreted to represent deposition by density-controlled river plumes in a freshwater lake (Stack *et al.*, 2018; Siebach *et al*., 2019; Sun *et al.*, 2019) and shows the dominant presence of thinly laminated mudstones. The Hartmann's Valley member is interpreted to have formed in a fluvial environment based on the presence of meter-scale trough cross-bedding with steep foresets (Fedo *et al.*, 2018; Gwizd *et al*., 2018; Siebach *et al.*, 2019). The Karasburg member is interpreted as lake deposits with some interbedded lake-margin facies (Siebach *et al.*, 2019). The Sutton Island member is made of heterolithic mudstone-sandstone (Fedo *et al*., 2017; Siebach *et al.*, 2019). The Blunts Point member formed as low-energy suspension from fallout in a lacustrine environment (Siebach *et al.*, 2019). Episodic lake drying and desiccation caused by fluctuating lake levels are interpreted in Hartmann's Valley through the Sutton Island members based on altered clay minerals found in drill samples (Bristow *et al.*, 2018). Halite is identified in these members based on correlation between Na and Cl observations in the Quela drill target in the Karasburg member (Achilles *et al*., 2018; Thomas *et al.*, 2019). The Sutton Island member also

shows the presence of dark-toned concretions and desiccation cracks indicative of wet-dry cycles associated with transient low lake levels (Sun *et al.*, 2018; Stein *et al.*, 2018; Haber *et al*., 2019; Siebach *et al.*, 2019). The Pettegrove Point and Jura members comprise Vera Rubin ridge (VRR; Fig. 1A), a nearly 250 m wide linear topographic feature that runs parallel to the northern foothill of the crater's peak, Mount Sharp, for nearly seven kilometers (Fraeman *et al.*, 2013, 2018). VRR was originally identified based on enhanced detections of hematite by the Compact Reconnaissance Imaging Spectrometer for Mars (CRISM) on the Mars Reconnaissance Orbiter (Fraeman *et al*., 2013). The stratigraphic members of VRR, Pettegrove Point and Jura, are compositionally similar to lower Murray formation strata. However, VRR is erosionally more resistant compared to the underlying Murray members, resulting in the ridge formation (Edgar *et al.*, 2018; Fedo *et al*., 2018; Fraeman *et al.*, 2018; Heydari *et al.*, 2018; Rivera-Hernández *et al.*, 2019; Siebach *et al*., 2019). The boundary between the two members is not observed as a clear hiatus, leading to the interpretation that the morphological differences between the two members are likely due to secondary (diagenetic) processes. VRR bedrock typically varies from bright to pale red or purple in color. These color differences may correspond to grain size (Johnson *et al.*, 2019). In situ images from the rover have shown that the topmost member of VRR (Jura), exhibits distinct color gradients. Decameter-scale gray patches are interspersed among the red bedrock, suggesting a possible redox relationship between these color units (Horgan *et al.*, 2019). The bulk chemical composition of VRR mudstones falls within the compositional range of Murray formation rocks, although there are variations in in situ geochemistry (Frydenvang *et al*., 2019 and Thompson *et al.*, 2019). VRR rocks show an overall decrease in Chemical Index of Alteration (CIA; defined as the molar ratio of Al_2O_3 and the sum of Al_2O_3, CaO, Na_2O, and K_2O; Nesbitt and Young, 1982), strong decrease in Li content, an increase in MnO content near the contact between the Pettegrove Point and Jura members (Frydenvang *et al*., 2019), and broadly elevated Na_2O concentrations compared to the underlying Murray formation (Thompson et al., 2019). Diagenetic iron-rich features, including concretions and nodules, are also reported in VRR (L'Haridon et al., 2019; David *et al.*, 2019).

Veins in the Murray Formation. Light- and dark-toned veins are observed across all members of the Murray formation and are found in complex associations with other diagenetic features (Gasda *et al.*, 2017; Nachon *et al.*, 2017; Fedo *et al.*, 2018; L'Haridon *et al.*, 2018; Stein *et al.*, 2018; Kronyak *et al.*, 2019; Siebach *et al.*, 2019; Sun *et al.*, 2019). Pahrump Hills shows the presence of light- and dark-toned veins throughout the stratigraphy (Nachon *et al.*, 2017; Kronyak *et al.*, 2019). The dark-toned veins enriched in Ca show the presence of fluorine and are interpreted as fluorite veins (Forni *et al*., 2017, 2019; Nachon *et al.*, 2017). The light-toned veins are

enriched in Ca and sulfur, and are interpreted as Ca-sulfate veins (Nachon *et al.*, 2017). Boron has been detected exclusively in light-toned Ca-rich veins and patches (Gasda *et al.,* 2017). Light-toned veins in Hartmann's Valley are encountered preferentially along vertical fractures within host rocks, frequently displaying central gaps within the veins and fibrous textures (L'Haridon *et al.*, 2018), but also displaying a concentration of Fe-rich and Mg-rich light-toned veins (L'Haridon *et al.*, 2018). The Karasburg member also shows the presence of light-toned Ca-rich veins (Gasda *et al.*, 2017) whereas the Sutton Island and Blunts Point members show the presence of abundant horizontal and sub-horizontal Ca-sulfate veins that are crosscutting finely laminated mudstone and are dispersed within concretionary bodies (Sun *et al.*, 2019; Rapin *et al.*, 2019).

3 Geochemistry of boron and lithium

3.1 Common borates and their formation conditions

B has a high affinity for oxygen and forms covalent boron-oxygen bonds in borates. On Earth, there are over 230 borate minerals present in the upper crust that originate by igneous, sedimentary, and metamorphic processes (Grew *et al.*, 2011; Grew, 2017). The type of borate formed is dictated by the amount of dissolved B in the solution and conditions including pH and temperature of the solution, degree of evaporation, the cations available in the fluid, and depth of burial of the borate formed (Christ *et al*., 1967; Birsoy and Özbaş, 2012). Here we focus on evaporitic borate deposits as they are the most relevant to Gale crater.

Common evaporitic borate minerals include colemanite ($Ca_2B_6O_{11}\cdot 5H_2O$), borax ($Na_2O.2B_2O_3.10H_2O$), kernite ($Na_2O.2B_2O_3.4H_2O$), ulexite ($Na_2O.2CaO.5B_2O_3.16H_2O$), probertite ($Na_2O.2CaO.5B_2O_3.16H_2O$), and hydroboracite ($CaMgB_6O_8(OH)_6\cdot 3H_2O$). Figure S1 shows a flowchart indicating formation conditions of common borates, constructed based on thermodynamic stability diagrams and chemical compositions (Christ *et al.*, 1967; Birsoy and Özbaş, 2012). It shows the chemical compositions, major cation category, deposit types, formation locations, and structural subdivisions of the common borates found on Earth (Christ *et al*.,1967; Birsoy and Özbaş, 2012). Boron may also be present as ions in inclusion fluids within host crystals. Possible fluid inclusion phases associated with borates and boric acid are discussed in section S4 in the supporting material. Although high contents of B and Li are commonly associated with hydrothermal activity on Earth (Seyfried *et al.*, 1984), these elements can also be liberated from relatively low temperature weathering of typically felsic igneous rocks (Risacher and Fritz., 2009).

3.2 Substitution and adsorption of boron

In addition to forming borates, B is also commonly found adsorbed to clay minerals (Hingston, 1964; Keren *et al.*, 1981; Keren and Mezuman, 1981; Keren and O'connor, 1982; Palmer *et al.*, 1987; Williams *et al.*, 2001) and amorphous materials (Biggar and Fireman, 1960; Bingham *et al.*, 1971; Evans and Sparks, 2008; Abu-Sharar *et al.*, 2014; Goldberg, 1997; Goldberg *et al.*, 1993; 2008). Borate ions can also substitute for other ions within minerals such as mica and illite (Stubican and Roy, 1962; Hingston, 1964, Couch and Grim, 1968), calcite, aragonite (Kitano *et al.*, 1978; Hemming *et al.*, 1995; Mavromatis *et al.*, 2015), and ettringite (a minor Ca-Al-Si sulfate solid solution hydrated evaporite mineral; Csetenyi and Glasser, 1993; Seryotkin *et al.*, 2018). Under relatively low-temperature conditions, $B(OH)^-_4$ anions are adsorbed onto the frayed edges (where Si—O and Al—O bonds have broken leaving positively charged sites: Couch and Grim, 1968) and between the silica layers of clay minerals (Stubican and Roy, 1962; Couch and Grim, 1968). This adsorption is rapid and followed by a slower diffusion of B into the clay structure (Couch and Grim, 1968). Above 60°C, B atoms can substitute for aluminum (Stubican and Roy, 1962) in clay mineral lattices (Stubican and Roy, 1962; Hingston, 1964). At the temperature range of 60-120°C, smectites begin to collapse into illite, which allows boron-aluminum substitution in the clay lattice (Burst, 1957; Eberl and Hower, 1976; You *et al.*, 1996; Williams *et al.*, 2001). The uptake of B within clay crystal structures depends on concentration, salinity of the solution, temperature, and interaction duration (Couch and Grim, 1968). Experiments show that B adsorption in clays and amorphous materials (and therefore the availability of B for incorporation into the mineral lattice) occur only in alkaline conditions (Keren *et al.*, 1981), at low temperatures (<120°C: Palmer *et al.*, 1987; Goldberg *et al.*, 1993; You *et al.*, 1996) and relatively high salinity (Lerman, 1966; Couch and Grim, 1968; Harder, 1970; Abu-Sharar *et al.*, 2014). Therefore the two ways B can go into solution from clay and amorphous materials are: 1) in high-water rock ratio conditions where the adsorbed B on clay mineral surfaces can be dissolved by neutral to acidic fluids and 2) in acidic conditions where B is released from the clay lattice on dissolution of the clay itself.

3.3 Substitution and adsorption of lithium

Li is more soluble than B in water; Li does not form salts as readily upon dehydration (although Li carbonates [zabuyelite: Miangping *et al.*, 2000] and Li silicates [jadarite: Stanley *et al.*, 2007] are reported associated with evaporites in playas in China and Serbia) and remains in the brine as dehydration continues (Hamzaoui *et al.*, 2003). Overall, Li is a conservative element that stays in solution and does not form salts easily (Risacher and Fritz., 2009). However, lithium is also commonly found adsorbed to or incorporated within the structure of terrestrial clay minerals (Greene-Kelly, 1955; Vine, *et al.*, 1980). The clays that adsorb Li on their surface and incorporate Li into their structures can be a notable source of Li (Vine and Dooley, 1980; Greene-Kelly, 1955).

Similar to the behavior of B, high water-rock ratio can dissolve Li adsorbed on clay minerals due to the high solubility of Li and dissolution of clays in acids can quickly remove the Li from the clay structure (Dalton *et al.*, 2016; Huang and Keller, 1971; Hall, 1977; Simon and Anderson, 1990). Although Li is not a universal proxy for clay content on Mars, it can indicate a relative change in the amount of clays in Gale crater (Forni, *et al.*, 2015; Frydenvang *et al*., 2019).

3.4 Terrestrial examples of B- and Li-rich brines

Although boron and lithium are predominantly associated with geothermal inputs on Earth (Li *et al*., 2019; Seyfried *et al.*, 1984), terrestrial brines can provide insight into B and Li systematics on Mars as the separation of the two elements in salt-forming environments appears to be common. In case of Gale crater, it is possible that the major water body and the groundwater was influenced by a hydrothermal system (or multiple systems) as large impacts produce long-lasting sources of heat below the surface, so Gale lake may have experienced early stage of hydrothermal activities (Schwenzer *et al.*, 2012). Systems with multiple sources of B and Li in a dry lake environment can act as an analog for better understanding the geochemistry of Gale crater.

Saline lake deposits on the Andean Plateaus show presence of B- and Li-bearing brines in internally drained, evaporative basins (Steinmetz, 2017). The brine composition is associated with local residual brines, solutions from weathered rocks, and parental lithology in addition to geothermal input (Steinmetz, 2017). However, the predominant sources of B in this case are reported to be inflow from residual brine and weathering of local rocks; in contrast, Li is associated with geothermal sources (Steinmetz, 2017). The evolutionary pathway of the evaporating water composition, in this case study, is interpreted to be determined by the extent of evaporation and the relative quantities of initial precipitated mineral phases such as calcite and sulfates (Steinmetz, 2017). Borates, sulfates and Li- and B-containing brines are reported in this region (Steinmetz, 2017). The brines contain up to 450 ppm of B and 125 ppm of Li (Steinmetz, 2017). Li-micas are also observed in this area; however, it is also stated these Li-micas are relatively rare findings in playa lake environments (Steinmetz, 2017).

The hyper-arid basins of Salar de Atacama in Chile also show the presence of Li- and B-rich brines in which the Li and B are determined to be sourced predominantly from varied locations of recharge corresponding to surrounding sub-watershed regions with possible geothermal inputs (Munk *et al.*, 2018). Mineral precipitation and brine evolution in this case study is also determined to be dependent on the composition of the source rocks, extent of brine mixing and evaporation (Munk *et al.*, 2018). Brines of Salar de Uyuni in the Southwest of the Bolivian Altiplano are also rich in Li and B (Haferburg *et al.*, 2017). These brines are slightly acidic to near-

neutral pH with Li and B concentrations of up to 2000 and 1400 ppm (Haferburg *et al.*, 2017). The source of B and Li in this case is also attributed to leaching of ancient evaporite from the catchment area during the evolution of the basin (Risacher and Fritz, 1991) which acts as a good analog for one of the possible enrichment methods of B and Li into evaporite veins of Gale crater as discussed in this study in Section 6.

4 Methodology

4.1 Data collection and processing

The ChemCam instrument suite onboard the *Curiosity* rover consists of a laser induced breakdown spectroscopy (LIBS) instrument and remote micro-imager (RMI). The LIBS instrument provides atomic emission spectra of targets (up to seven meters standoff distance) by focusing a pulsed 1067 nm laser, with a 350–550 µm diameter spot size, creating a plasma from the ablated surface (Maurice *et al.*, 2012; Wiens *et al.*, 2012). Together with color images from the Mastcam imaging suite (Malin *et al.*, 2010) and Mars Hand Lens Imager (MAHLI; Edgett *et al.*, 2012), the RMI allows for visual identification of features and the geologic context for each observed point (Le Mouélic *et al*., 2015). Sampling frequency is dependent on the rover's resources and its topographic accessibility to the sampling area. Although efforts are made to collect bedrock and diagenetic features, including veins, at each rover location, compared to sampling performed for chemostratigraphic studies on Earth, rover sample sets are less systematic. The Martian data interpretations are therefore subject to some sampling bias.

ChemCam data are acquired by lasing the area under investigation in either a linear or gridded array with a typical spacing of 1–2 mrad that spans approximately 15 mrad (Wiens *et al.*, 2015). Each ChemCam analysis point is typically hit by 30 laser pulses and average chemical compositions are calculated after discarding the data from the first five spectra due to the pervasive dust coating on the rocks (Wiens *et al.*, 2013; Clegg *et al.*, 2017). Major element concentrations of Ca sulfate veins and surrounding rocks are determined using multivariate analytical methods including partial least squares for the ChemCam spectra (Wiens *et al.*, 2013; Clegg *et al.*, 2017). Sulfur is not typically quantified by the ChemCam team, as its emission lines are weak in the spectral range covered by this instrument. Because of this, Ca-sulfates are identified by the presence of strong enrichments of Ca (e.g., > 20 wt. % CaO) along with the identification of a S peak. The calibration for B is described by Gasda *et al.*, (2017) with a limit of detection (LOD) of ~100 ppm. The calibration for Li is provided using a univariate model with an LOD of 5 ppm and root mean square error (RMSE) of 5 ppm (Payré *et al.*, 2017). The data used for plotting the Li concentrations can be found in the PDS Geosciences Node Data and Services repository (https://pds-geosciences.wustl.edu/missions/msl/chemcam.htm) and the corrected Li

concentrations can be found in a Zenodo data repository (Das, 2020: http://doi.org/10.5281/zenodo.3877377). For boron, the presence of iron can limit detection. The majority of ChemCam targets contain >18 wt.% FeO_T (Gasda *et al*., 2017; Mangold *et al.,* 2017). ChemCam data shows unresolved neutral atomic B emission lines at 249.75 and 249.84 nm. An Fe II line interferes with the B feature at 249.96 nm (Sansonetti and Martin, 2005; Gasda *et al.*, 2017). Hence, B can only be detected in low-Fe targets, and so far, only in Ca-sulfate veins. New targets for this study were selected based on low Fe content of the target (FeO_T < 13 wt%), reasonable total emission of the ChemCam spectra (>5 x 10^{13} photons), and targets within four meters. The B peak area (labeled on Figure 1B) is corrected for the expected peak area ±2σ uncertainty of the very weak Ca III emission line at 249.84 nm as determined by method blanks (described in supporting information document by Gasda *et al.*, 2017,). The detection of B is determined by fitting the B and iron peaks in the feature and identifying targets with non-zero B peak areas after the calcium III correction. In Gasda *et al.* (2017), most of the targets have >3σ certainty of B detection.

4.2 Subtraction of bedrock component from Ca-sulfate veins

The LIBS laser often hits an area consisting of both bedrock and Ca-sulfate (Nachon *et al.*, 2014), resulting in a mixed composition (Figure S2.1). To understand the trends in soluble elements of the veins, the contribution of the bedrock must be removed from these mixed observations. The ratio between SiO_2 in the bedrock and veins is used to determine the percentage of bedrock contribution in these observations. For each vein or partial vein target, nearest bedrock targets are identified. The composition of a maximized number of nearest available bedrock targets are averaged to determine an average bedrock composition. The average bedrock composition for all the major oxides and Li is multiplied by the vein-observation-to-bedrock SiO_2 ratio and is then subtracted from the vein observation. The bedrock-subtracted vein compositions are then renormalized to an average oxide sum of an 'ideal' Ca-sulfate target to obtain the corrected oxide and Li values. This method has not been applied for B, as B cannot be measured in the bedrock due to the high FeO_T content of the bedrock. The ideal Ca-sulfate targets are compositionally close to anhydrite (Table S2.1), and are chosen based on the lack of SiO_2, Al_2O_3 and TiO_2, as these elements are typically the least soluble in vein-forming fluids and therefore should not be present in pure Ca-sulfate veins. If the true composition of the veins is gypsum or basanite (presence of basanite veins has been confirmed in Gale crater by Rapin *et al.,* 2016) , this renormalization method may impart a small error to the data, increasing the absolute amount of Li detected in the veins by up to 8.5 rel.%, much less than the expected error due to uncertainty (Table S2.2). The relative amount of Li within a vein is expected to remain constant. Error is calculated using linear propagation of uncertainty (section S2) based on the RMSE accuracy of

the major oxide model (Clegg *et al.*, 2009). Since a single bedrock point is used for error propagation rather than an average of points, this method is the most conservative method of estimating error. As more bedrock targets are averaged as part of the correction, the error is expected to decrease by the square root of the number of samples used to calculate the mean. More details about the correction method and error propagation can be found in section S2 in supporting information.

5 Results

Boron was detected in 21 new vein targets (after detections reported by Gasda *et al.*, 2017) with 33 single-point observations (with a range of one to four B observations per target). Boron concentrations in the 21 vein targets range between ~100-150 ppm, which is comparatively lower than the up to ~300 ppm detections in the lower units described by Gasda *et al.*, (2017). Table S3.1 lists the target names, analysis sol number, ChemCam observation point number, corrected B peak area, vein type, and the host unit names of all B-containing targets. Corrected Li concentration of all vein targets vary between 5 and 65 ppm; these results can be found in the supporting data file named "Corrected-Li-ppm.xlsx". After correcting for rock content in the vein observations, Ti, Al, Fe, Na, K, Mg, Sr, Ba, and Rb concentrations are below the quantification limit for the targets. All the data used throughout this study (ChemCam data collected between sol 0-2311) can be found in supplementary excel file titled "All data-sol-0-2311.xlsx".

5.1 Morphology of sulfate veins

On VRR, B is observed in both thick and thin veins and Ca-sulfate patches that are a few centimeters in width and irregular in shape (patches in some cases appear to be broken or partially exposed veins). Boron is found in veins that are more erosionally resistant than surrounding host rock as well as in veins exposed flush with the bedding plane surface (Figure 2C and D). A few thicker, patchy light-toned targets, possibly representing remnants of eroded veins, also show B presence (Figure 2E). Boron is detected in two different float rock targets (Figure 2F and G): Askival, which is a silicified feldspathic cumulate rock (Bridges *et al.*, 2019) with a Ca-sulfate rim (CaO abundance of 30.8 wt % and clear S emission peaks), and Blair Atholl, which is a Ca-rich (twice targeted with 34.7 and 33.6 wt. % CaO) light-toned float rock. These observations show that B is detected in light-toned veins with no preference for morphology or rock type.

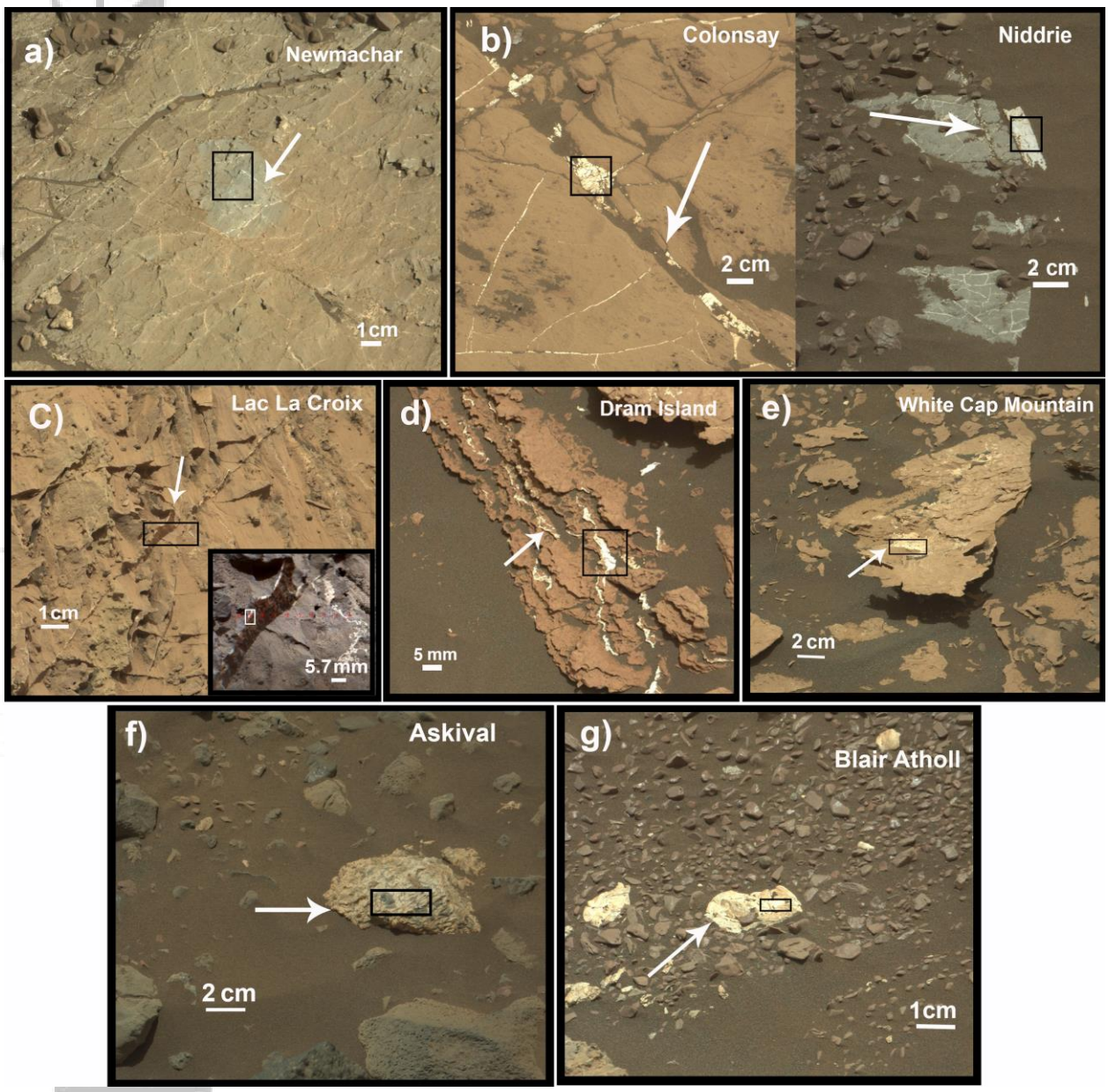

Figure 2. Morphologies of light-toned materials where boron has been observed in VRR. **a)** Thin veins cross-cutting each other in target Newmachar shown by white arrow (sol 1965 with B detected in point15). MastCam image ID 1965MR0102770000901670E01. **b)** Truncation of thin veins against thicker veins shown by white arrows in Colonsay (left, sol 2012 with B detection in point 6, MastCam image ID: 2012MR0105980000902590C00) and Niddrie (right, sol 2250 with B detection in point 4 and 5 MastCam image ID: 2250MR0120360010106377C00). **c)** Erosionally resistant veins in Lac La Croix shown by white arrow (sol 2048 with B detection in point 9). MastCam image ID: 2048MR0108370000903354C00. **d)** Veins running across bedding planes in Dram Island shown by white arrow (sol 1641 with B detection in point 5). MastCam image ID: 1641MR0105920000903652C00. **e)** Patchy white toned material observed in target White

Cap Mountain shown by white arrow (sol 1707 with B detection in point 5). MastCam image ID: 1707MR0089010000803320E01. **f)** Askival, a silicified feldspathic float rock shown by white arrow (sol 2015 with B detection in point 2). MastCam image ID: 2016MR0106360160902714C00. **g)** Blair Atholl, a Ca-rich light-toned float rock shown by white arrow (sol 2235 with B detection in point 2, 3, 4, and 5). MastCam image ID: 2235MR0118800000106144C00.

Figure 2B shows two sets of textural relationships where, based on the cross-cutting relationship, the veins hosting B appear to have formed in different fracturing events from surrounding veins. The target Colonsay in Figure 2B (left) shows that the vein hosting B is cross-cut by another vein in the top-left corner. The thinner veins on the bottom left truncate against the thicker, boron-containing vein. Although the exact sequence of vein formation is unknown, the cross-cutting vein on the top left corner likely formed after the one in the middle. In case of the target Niddrie, (Figure 2B right) a similar observation is made where the thinner veins in the left side truncate abruptly against the thicker vein. This occurrence may suggest that different fracture and fluid flow generations brought in fluids with varying composition and may add to the explanation of detecting B in only some spots, however, the absence of B detection does not indicate complete absence of B due to the ~100 ppm detection limit of boron. The cross-cutting features seen from the surface only provide a limited picture of the three-dimensional relationship of the veins under the surface.

Vein textures and crystal habits (Figure 3) can shed light on potential formation mechanisms and crystal growth histories. Tooth-like textures with a central discontinuity can be observed in the vein in Figure 3A and a fibrous habit of the white infill material can be observed in Figure 3B. Similar textures observed in veins in lower stratigraphic units have been interpreted to have formed by a repetitive fracture filling process called crack sealing (Hilgers and Urai, 2002; Kronyak *et al.*, 2019). In the targets Long Porcupine (Figure 4A) and Milton Ness (Figure 4B), light-toned veins contain variably sized dark-toned features within their matrix. For target Long Porcupine, two veins intersect each other orthogonally. Both veins have been analyzed, but only one vein shows the presence of B. A similar textural setting is observed in Figure 4B where the target shows multiple

veins with varying morphologies. The B-containing vein (middle) shows the presence of small dark features (similar to features observed by L'Haridon *et al*., 2019).

Figure 3. Vein textures observed by Remote Micro Imager. **a)** Tooth-like texture in target Blackhoof (sol 2045). Points 3 and 4 show presence of boron. MastCam image ID: 2045MR0108220020903332C00. (**b)** Fibrous texture visible within vein (sol 2012). Boron was detected in point 6. Darker material observed in sections of the

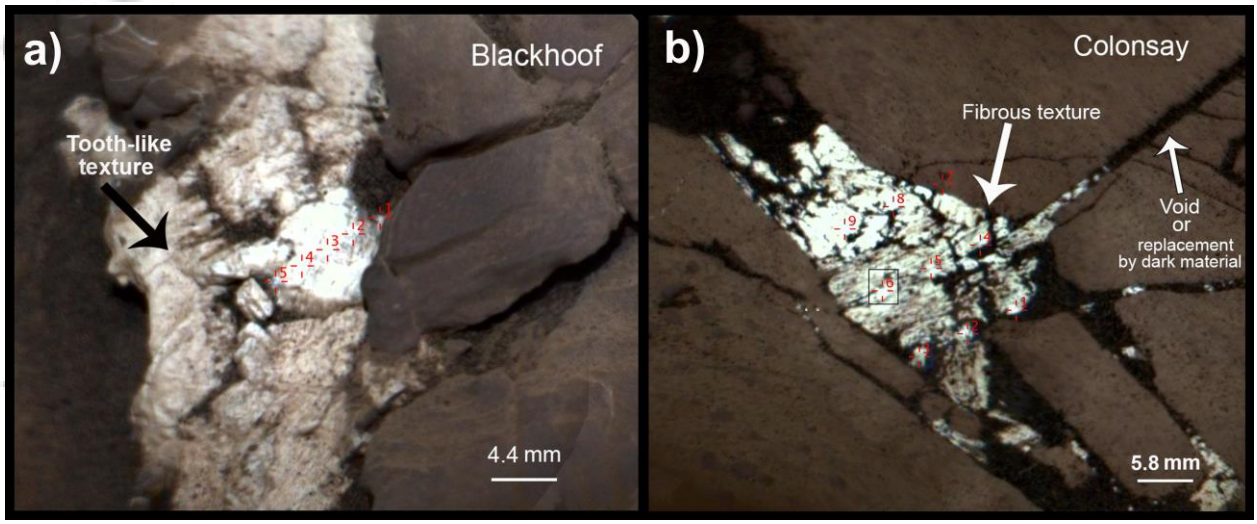

thick and orthogonal thin veins may be a void formed by erosion of the vein or replacement by dark-toned features. MastCam image ID: 2012MR0105980000902590C00.

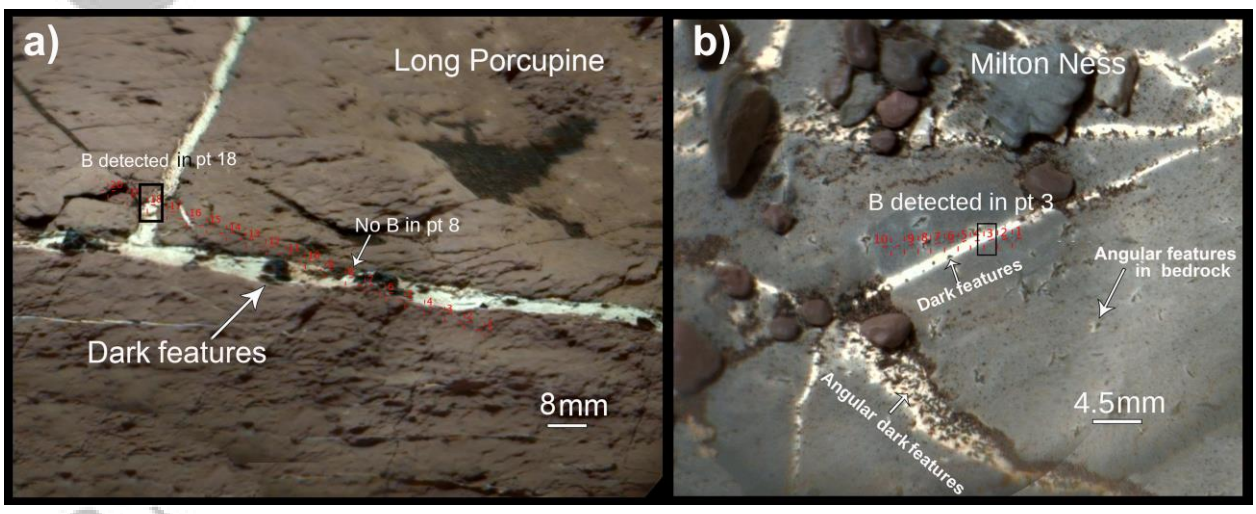

Figure 4. Veins containing dark features. **a)** Light toned veins in Long Porcupine (sol 1552) show an orthogonal intersection with dark-toned features in one side. MastCam image ID: 1552MR0079700000800082E01. **b)** Light-toned veins in Milton Ness (sol 2218) showing different densities and morphologies of dark-toned features. Angular features are also observed in the host bedrock of the veins. MastCam image ID: 2218MR0117520000105898C00.

The intersecting vein in the bottom left area also shows dark features but these are angular in shape and significantly higher in numbers. Angular features are also observed in the surrounding bedrock. However, the lack of B observation is not an indicator of the element's absence; it may be present at a concentration just below the limit of detection.

5.2 Stratigraphic detections of boron and lithium in veins

Figure 5 shows bedrock-corrected Li concentrations of the Ca-sulfate veins (pink) compared to nearby bedrock (black). All errors described in this section, unless otherwise stated, are 2σ standard error. The corrected Li values in the veins below the contact between the Blunts Point and Pettegrove Point members (Li peak 1 between -4231m to -4221m in Figure 5) have an average of 21 ± 5 ppm. Values below the contact between Pettegrove Point and Jura members (Li peak 2 between -4191m to -4181m in Figure 5) have an average of 21 ± 5 ppm). Both locations have a significantly higher average of Li abundance than the average corrected Li abundance of all the veins in Gale crater (12 ± 2 ppm). Lithium has a significantly lower abundance in the veins of Jura member (with an average of 8 ± 2 ppm) compared to the veins in the peak Li locations in Pettegrove Point and Blunts Point, and slightly lower than the average Li concentration of all Gale veins (11 ± 2 ppm). The concentration of Li is relatively lower in the Jura bedrock with an average of 8 ± 1 ppm compared to the average Li concentration of all bedrock targets (average of 13.2 ± 0.3 ppm). The distribution of corrected Li values in the veins for each stratigraphic unit is statistically different from the distribution of the measured Li values of the surrounding bedrock (see section S2 in supplemental information for detailed discussion of error).

The stratigraphic units where ChemCam detected veins (>20 wt% CaO; <13 wt% FeO_T) and the frequency of B detections within vein targets is shown in Figure 6 and Table S3.2. Figure 1 shows B detections throughout the traverse beginning in Yellowknife Bay formation, but no detections in the remaining Bradbury group or lower Murray formation. B detections increase through the Pahrump Hills (7 detections), Hartmann's Valley (11 detections), and Karasburg (27 detections) members and decrease in the Sutton Island member (13 detections). Although veins were often targeted in the Blunts Point member, the B detection frequency decreases drastically (one target in this unit was below the 2σ threshold for detection). B detection frequency increases in the upper Pettegrove Point (11 detections) and Jura (16 detections) members. The detections appear to be concentrated toward higher elevations in VRR in the Jura member (between -4171 to -4142 m). The increased detections in Pettegrove Point and Jura members contrast in the detection frequency between the Blunts Point member and both VRR members.

Figure 6 also shows a comparison between B detection frequency and average corrected Li concentration of the veins. This plot shows high Li concentration of the veins is only observed at units with low B detection frequency across the rover's traverse. This potential link between Li concentration of the veins and relative B peak area is further illustrated in Figure 7. Figure 7A shows the B observation frequency every 10 m elevation and possibly has a weak inverse relationship with the corrected Li concentration of the veins. Figure 7B shows a similarly weak inverse relationship between relative B peak areas averaged over every 10 m elevation and the average corrected Li concentration of the veins. A curve defined by power law ($f(x) = Ax^B$) is fitted through both scatter plots and illustrates the potential relationship (e.g., that of a phase change, whereas one element leaves solution through crystallization, and the other is concentrated in the brine) between the two elements. The R^2 values suggests the relationship between B and Li weakly follows the power law. These fitted curves are only for illustrative purpose as they are constructed using only non-zero data. Hence, the power law relationship shown in Figure 7 does not fully describe the system. The 2σ Spearman's correlation coefficient between B observation frequency and average Li concentration of veins per 10 m is -0.53 and between B average peak area and Li concentration of veins per 10 m is -0.48. These values indicate a weak negative correlation between B observation and average Li concentration of veins and between B average peak area and Li concentration of veins per 10 m. In summary, the relationship between Li and B is weak in the limited dataset and a power law relationship only partially describe the system; chemical modeling of all the trace elements is likely required to build a full picture of the groundwater system in VRR.

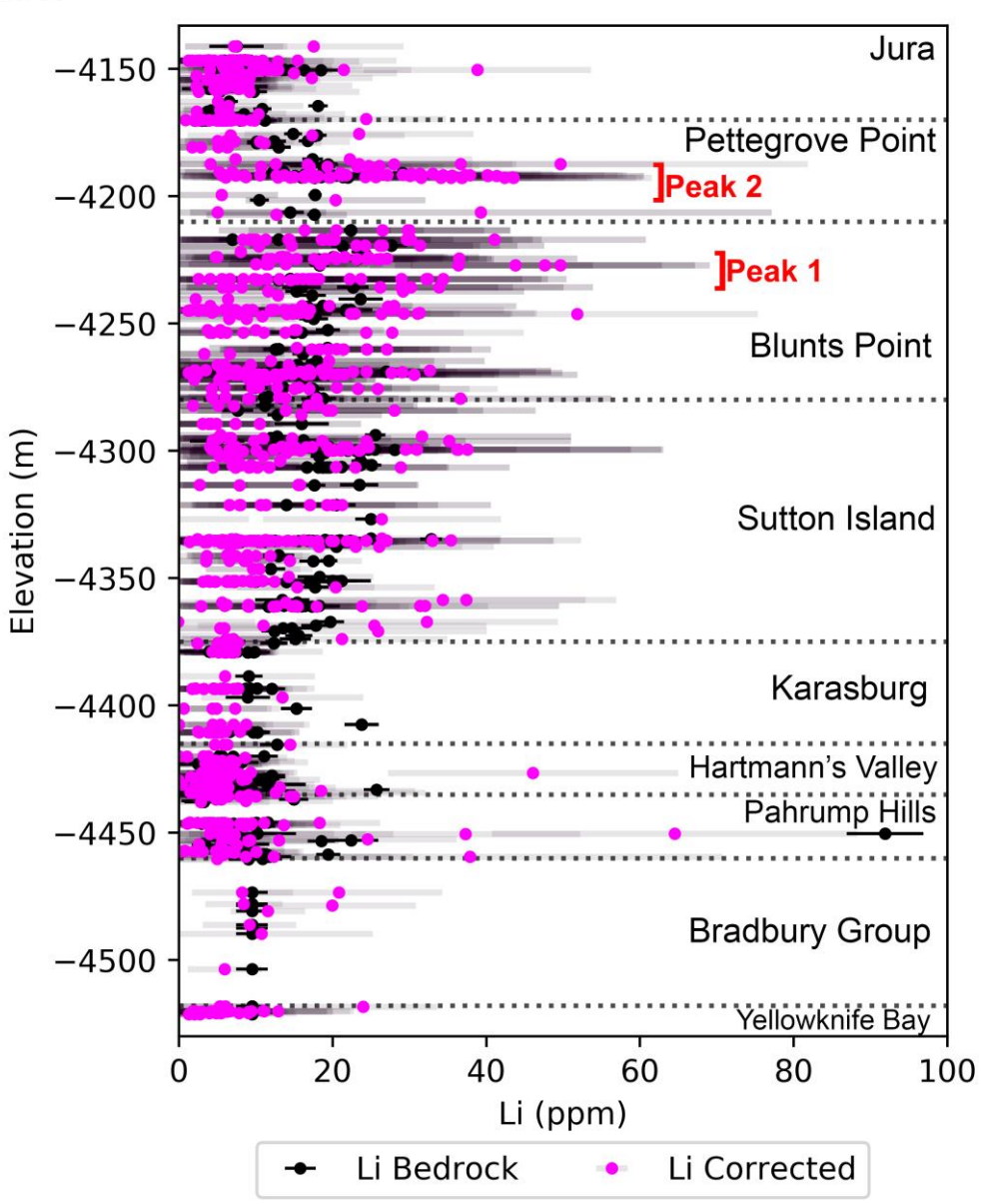

Figure 5. Plot showing the corrected Li concentration of the high-Ca veins against elevation, compared with the Li concentration of the surrounding bedrock. Pink filled circles show the corrected Li concentration of the veins. Black filled circles show the Li concentration of the surrounding bedrock. Locations with increased concentration of Li are visible right below the contact between Blunts Point and Pettegrove Point members (Peak 1) and below the contact between Pettegrove Point and Jura members (Peak 2). Errors propagated during the correction calculations are shown as grey bars. Errors associated with the original vein and bedrock compositions are shown as thin black bars.

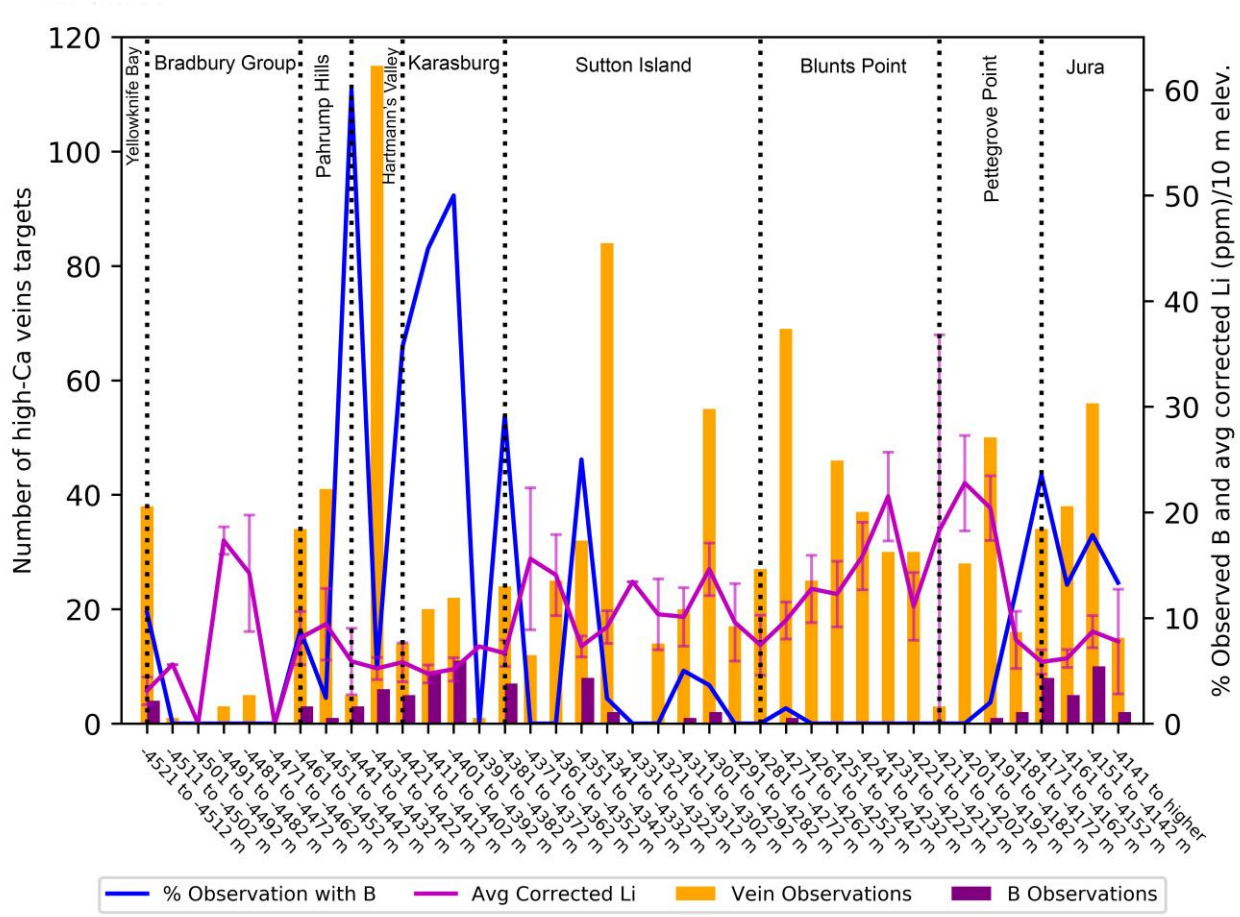

Figure 6. Histogram showing the distribution of Ca-rich veins in Gale Crater throughout Curiosity's traverse (sols 0—2311), frequency of Ca-rich veins with boron, and comparison of Li concentration of veins with relative frequency of boron detections in veins. The orange bars show the number of Ca-rich (>20 wt% Ca) targets (left axis) in intervals every 10 m elevation (horizontal axis). The purple bars show the number of Ca-rich veins containing boron. The blue line indicates the percentage of veins with boron out of all analyzed veins at that elevation (right axis). The average corrected Li concentrations of the veins are plotted as a magenta line (right axis) and 2σ standard errors bars are shown. The vertical dotted lines separate the different stratigraphic units of Gale Crater. The units shown are the Bradbury group and members of the Murray formation. Yellowknife Bay formation is a part of the Bradbury group, but it is shown separately because of the boron observations made there. Ca-rich veins occurred much less frequently in the rest of the Bradbury group, with no boron observations. Comparison of the pink and blue lines in the plot indicates a negative correlation between the frequency of B detection in the veins and the concentration of Li.

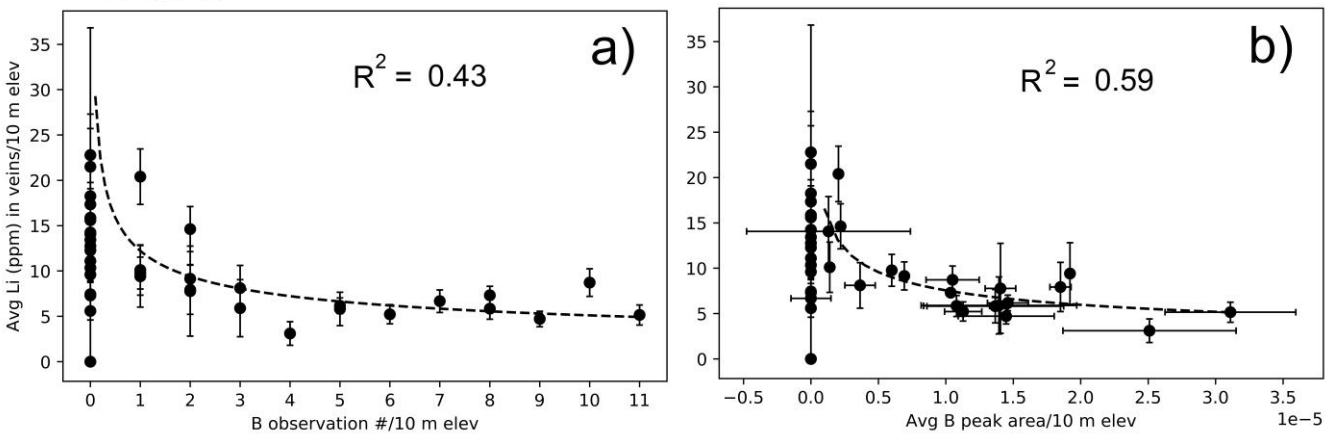

Figure 7. Average corrected Li concentration of the veins with B detection frequency and average B peak areas with 2σ standard error bars. a) A weak inverse correlation between B detection frequency every 10 m elevation (x-axis) and the average Li concentration of the veins (y-axis) with an R^2 value of 0.43. The Spearman's correlation coefficient between B observations frequency and average Li concentration of veins per 10 m is -0.5. b) A weak inverse correlation, illustrated by the black dashed power law curve based on non-zero data points, between B peak areas averaged over 10 m elevation bins (x-axis: the B peak area average values are of the order of magnitude ~10^{-5} which is shown as 1e-5 on the right end of the x-axis of this plot) and average Li concentration of the veins (y-axis), with an R^2 value of 0.59. The Spearman's correlation coefficient between B average peak area and Li concentration of veins per 10 m is -0.48. For Figure 7B, the average B peak areas shown at zero are below the detection limit. In some cases, where the average peak areas are more than zero, but error bars cannot be seen, the error bars are smaller than the plotted data points.

6 Discussion

6. 1 Relationship of boron and lithium in calcium-sulfate veins

We see no direct evidence that indicates the exact sequence of events that resulted in B and Li enrichment in veins of VRR. We hypothesize a possible sequence of events in Gale crater based on observations made on Earth and supporting observations made in Gale crater. The sequence of events discussed in the following sections is only one of the possible pathways and at this stage without geochemical models to support them, provide a useful working hypothesis but are speculative at best.

In addition to B, the Ca-sulfate veins show the presence and variation in concentration of another fluid mobile element: Li. The boron-containing Ca-sulfate veins show an increase in Li in Sutton Island, Blunts Point, and lower Pettegrove Point members (Figure 6) but a decrease in veins of upper Pettegrove Point and Jura members. Figures 6 and 7 show that with increase in frequency and relative abundance of B, the abundance of Li in the

veins decreases. This relationship could partially be a result of preferential separation of B from Li during precipitation of borates based on the power law fitted to data in Figure 7. In the case of a brine, with increasing dehydration, Li remains in the brine as other salts precipitate out due to the conservative nature of Li (Risacher and Fritz., 2009; Hamzaoui *et al*., 2003). In Gale crater, progressive dehydration of the groundwater would cause B to precipitate as a borate, leaving Li in the brine. The remnant Li-rich brine may have moved down gradient from the borate-bearing veins along VRR (refer to elevations in Figures 6 and 7), producing the observed spatial and stratal separation of the elements.

The Li patterns of the veins across the stratigraphy of Gale crater do not follow the Li concentration patterns of the surrounding bedrock (Figure 5). The average corrected Li concentration in the veins is relatively low in the lower Murray members (Pahrump and Hartmann's Valley) and begins increasing in mid-Murray members (Karasburg, Sutton Island and Blunts Point) with a sharp drop in the Pettegrove Point member (Figure 6). This pattern of Li concentration corresponds to an opposite pattern in the detection frequency of B across the traverse. Members with low Li concentration (Pahrump and Hartmann's Valley in lower Murray; upper Pettegrove Point and Jura in upper Murray) correspond to a higher detection frequency of B in the veins and members with high Li (Murray members: Karasburg, Sutton Island and Blunts Point) correspond to low detection frequency. For example, in the upper elevations of Pettegrove Point (Figure 6) a sharp drop in Li concentration is observed over the same elevation range as a sharp increase in the number of B detections. This inverse correlation of Li concentration of veins and B detection frequency could possibly reflect a classic progression of evaporation based on relative solubilities of Li and B (Dalton *et al.*, 2016). Li exists in solution commonly as Li ions; however, it can precipitate as Li chloride when the solution reaches saturation with respect to Li. Li chloride is two orders of magnitude more soluble than B in solution as boric acid at 0°C (Dalton *et al.*, 2016).

Terrestrial studies show that Li is adsorbed to clays (Greene-kelly, 1955; Starkey, 1982) and although it is not a universal proxy for clay content, it can be is used as an indicator of relative clay amount across VRR. The lower levels of Li in the bedrock (Frydenvang *et al.*, 2019) suggest reduced clay content in the Jura member. This is confirmed by the relatively low abundances of phyllosilicates detected in VRR bedrock compared to surrounding units by X-ray diffraction with the CheMin instrument (Bristow *et al.*, 2018; Rampe e*t al.*, 2019). As discussed in Section 3.2 and 3.3, B and Li adsorbed to clays can be incorporated into the clay structure as well as adsorbed by on clay surfaces (Frederickson and Reynolds, 1960; Lerman, 1966; Harder, 1970; Perry, 1972; Karahan *et al.*, 2006), although B cannot be detected in the clay-rich bedrock due to its FeO_T content and

interference with the B measurements (Gasda *et al.*, 2017). Boron and lithium can only be re-mobilized from clays through two ways: 1) adsorbed B and Li on clay mineral surfaces can be dissolved by neutral to acidic fluids in high water-rock ratio conditions; 2) boron and lithium trapped within clay lattice can be only be released into solution through dissolution of the host clay minerals. Enrichment of B and Li in Ca-sulfate veins after recirculation of fluids may have been a result of varying degrees of both these processes. In Figure 7, we observe only a weak correlation between B and Li, which may suggest that more than one process may have been responsible for the enrichment of B and Li.

Within the host bedrock, Li is reported to follow the morphology of the ridge rather than the elevation and is observed to be elevated in the Sutton Island, plateauing in the upper Sutton Island, decreasing towards Blunts Point, increasing again in the upper Blunts Point and strongly decreasing in the mid-Pettegrove Point to Jura members (Frydenvang *et al.*, 2019). In the Jura member, the Li concentration of both bedrock and veins drops significantly (Figures 6 and 7). However, the drop in Li concentration of the veins and the bedrock are likely caused by different factors. Notably, in terrestrial borate rich evaporites such as salars in the Bolivian and Chilean Andes (Risacher and Fritz, 2009), Li remains in the brine while B-salts precipitate. Thus, the Li concentration of veins might reflect the extent of dehydration of the diagenetic fluids beyond the solubility of Li-salts, while the Li concentration of the bedrock is controlled by the clay content of the bedrock.

6.2 Possible timing and mechanism of boron and lithium emplacement

6.2.1 Murray sections below VRR

In specific locations of the Murray formation, B is detected in light-toned Ca-sulfate veins. The frequency of B detection does not correlate with the frequency of Ca-sulfate targets analyzed throughout the upper Murray formation, so there is no fixed percentage of B in the veins. As discussed in Gasda *et al.* (2017), it is possible that later groundwater fluids remobilized pre-existing unobserved local B-rich evaporite layers in the immediate vicinity while they were circulating through the cracks in the Murray to form the Ca-sulfate veins and eventually redeposit the dissolved B as isolated borate grains in crevices of the veins located close to the primary evaporites. Based on the observation of truncating veins (Figure 2), fibrous and tooth like textures of vein fillings (or cements) (Figure 3), and veins containing dark features (Figure 4), it may also be interpreted that veins formed in multiple stages. More than one fluid flow event could have occurred, moving fluids through the cracks with varying compositions as (as is interpreted for veins with similar morphologies; Kronyak *et al.*, 2019; L'Haridon *et al.*, 2019). These events, which may have taken place as stratally isolated events, may have cause differences in fluid conditions between veins and the diversity of lithology through which the veins have

formed. These differences may be responsible for the variation of the frequency of B occurrence and its concentration.

Other studies of Ca-sulfate veins and clay minerals in lower Murray members (Pahrump Hills, Hartmann's Valley, and Karasburg) suggest an upper temperature limit of ~60°C (Nachon *et al.*, 2014, 2017; Vaniman *et al*., 2014; Schwenzer *et al.*, 2016; Rapin *et al.*, 2016) which suggests that the extent of burial depth in these members is relatively minimal. With minimal burial depths, the formation of initial borate phases that require higher temperature and pressure for their formation can be ruled out.

Increased frequency of B detection in the lower Murray (members Pahrump Hills, Hartmann's Valley, and Karasburg, and the lowest strata of Sutton Island) may point towards the initial availability of B-rich evaporites in the bedrock. Increased frequency of B detection correlates with the detection of chloride salts (eg. Forni *et al.*, 2017; Thomas *et al*., 2019), Mg sulfates (Rapin *et al.*, 2019), the presence of desiccation cracks (Stein *et al.*, 2018), and altered clay minerals (Bristow *et al.*, 2018). These occurrences suggest elevated evaporation and support the possibility of pre-existing B-rich evaporites in the bedrock. The lack of observation of the B in upper strata of Sutton Island may suggest that the fluids which emplaced the B in veins were short lived relative to the timescales of diffusion and circulation rates of borate in the groundwater. The decrease of B detections upslope into the Sutton Island member may represent the water table level at the time of B emplacement. No evidence for these local B-rich evaporites in the bedrock have been found yet, however it may be possible that these evaporite layers were very thin, resembling a crust (Lowenstein *et al.*, 1985), and may have completely dissolved and been carried away by fluids during the remobilization process. (Borates and associated temperatures are shown in Figure S1; borate phases in Ca-sulfate veins of Gale crater are discussed in section S4.)

6.2.2 VRR

Vera Rubin ridge was initially deposited in a lacustrine setting as evidenced by its thin laminations similar to the Blunts Point unit, which later underwent secondary complex sets of diagenetic events (Edgar *et al.*, 2018; Fedo *et al*., 2018; Fraeman *et al.*, 2018; Heydari *et al.*, 2018; Rivera-Hernández *et al.*, 2019; Siebach *et al*., 2019). Presence of minerals such as jarosite and akageneite in VRR suggest that the fluids associated with the diagenetic events may have been acidic (Morris, *et al.*, 2019; Rampe, *et al*., 2019). Our hypothesis, explained below, is that these diagenetic events may have mobilized B and Li out of clays in the VRR host rocks. A later set of groundwater events took place after the lithification and fracturing of VRR bedrock caused formation of Ca-sulfate veins (Nachon *et al.*, 2017; Kronyak *et al.*, 2019; Sun *et al.*, 2019). This fluid flow event may have

recirculated previously liberated B and Li from the clay minerals into the Ca-sulfate veins in VRR, and our second hypothesis is that the B and Li became separated from each other during the last stages of calcium sulfate precipitation and groundwater desication. The stages and timing between the initial set of diagentic events that altered VRR and the later fluid flow events that formed the sulfate veins are unknown.

The observations of the sedimentary facies of VRR suggest that, prior to the diagenetic fluid events that altered it, VRR was chemically and mineralogically very similar to other lacustrine Murray sediments (Fedo *et al*., 2018; Siebach *et al*., 2019). Hence, much like the lower Pahrump Hills region, very little B was likely present within the groundwater prior to the diagenetic event that altered VRR. Directly below VRR, the Blunts Point member unit does not show any evidence of a lake margin or evaporitic environment; rather, it shows evidence of a low-energy lacustrine environment. The lack of other evidence such as desiccation cracks, altered clay minerals, or evaporitic materials (e.g., chloride salts: Thomas *et al.*, 2019) is consistent with a lake rather than a lake-margin environment. While Pettegrove Point and Jura also show increased presence of chlorides (Thomas *et al.*, 2019), these observations might be explained by alteration of the bedrock minerals during the diagenetic event, resulting in formation of Cl-rich crystalline akaganeite in upper VRR (Rampe *et al.*, 2019), rather than pre-existing layers of evaporites. Moreover, both members of VRR and the Blunts Point member also show evidence of a low-energy lacustrine environment (Fedo *et al*., 2018; Siebach *et al*., 2019) which makes it difficult to explain the presence of primary boron-rich evaporites. Therefore, we suggest there is not enough evidence for evaporites near Blunts Point or VRR to be the source of the boron. Rather, the evidence points to B likely being sourced from the surrounding rocks during the diagenetic event.

Results from the X-ray diffraction instrument CheMin indicate the presence of gray hematite, ferripyrophyllite, and opal-CT, suggesting that the diagenetic fluids were warm; the presence of minerals jarosite and crystalline akaganeite observed in two drill holes in VRR suggest that the fluids were acidic (Morris, *et al.*, 2019; Rampe, *et al*., 2019) at least at one point in time. Note that acidic events also might be later in time than circumneutral diagenesis, based on the age dating of the Mojave2 drill core sample at Pahrump Hills (Martin *et al.*, 2017). The lack of depletion of soluble major elements argues against a strong or prolonged acid interaction (Frydenvang *et al*., 2019), but might indicate an ion-exchange process through contact with a saline fluid (e.g., Nir *et al.*, 1986; Gast *et al.*, 1971). The presence of warm and (at least briefly) acidic conditions on higher elevations of VRR would explain the decrease in clay content, as acids are known to readily dissolve clay minerals (Huang and Keller, 1971; Hall, 1977; Simon and Anderson, 1990). The exact timing of the first set of diagenetic events at VRR and the Ca-sulfate vein forming events and the relationship between the two events is unknown, however,

it is known that Ca-sulfate vein formation took place after the lithification of the Stimson formation (e.g., Frydenvang *et al.,* 2019). Boron and lithium were possibly deposited in the Ca-sulfate veins during the second set of fluid circulation events and the relative solubilities of the elements defined the sequence of mineral precipitation and evaporite formation in the veins. Calcium sulfate is one order of magnitude lower in solubility than boric acid (sassolite) and sodium tetraborate hexahydrate (borax), and three orders of magnitude lower than solubility of Li chloride at 0°C (Dalton *et al.*, 2016). Calcium sulfate begins to crystallize at fluid temperatures as high as 40°C-60°C and will continue crystallizing at lower temperatures (Hardie, 1967). After extensive crystallization of calcium sulfates, the water-to-rock ratio is expected to decrease, which would cause the resultant fluid to be rich in more soluble elements such as B, Li, and Cl. As the fluid evaporates further, B would crystallize as borate salts, while Li would remain in solution due to its inherent higher solubility even at low temperatures (Dalton *et al.*, 2016). Sodium and chlorine precipitate as chloride salts after borates. The acidic environment in Jura (Morris, *et al.*, 2019; Rampe *et al.*, 2019) may have affected the type of borate that crystallizes out of the diagenetic fluids in Gale crater. On Earth, sassolite, a borate that forms in acidic environments, is reported in dry lakes of Southern California (Allen and Kramer, 1957; Smith *et al*., 1958). Therefore, it is possible that sassolite may have formed as a secondary borate in acidic conditions on VRR (Figure S1). After the crystallization of borates, the remaining fluid is still expected to contain Li as it does not form salts easily. The remaining Li-rich fluid would have moved down gradient to the underlying stratigraphic units (peaks 1 and 2 labeled in Figure 5) and pooled on top of impermeable layers. This brine is unlikely to move through lower layers due its extremely low water to rock ratio. This sequence of events is one potential explanation for the separation between B and Li after prolonged dehydration of the brine resulting after Ca-sulfate formation. In summary, VRR started out similar to the underlying lacustrine Murray units; however, VRR underwent a diagenetic event altering its mineralogy and chemistry. This diagenetic event possibly liberated both B and Li from clay minerals in VRR. A later fluid flow event may have remobilized the B and Li and deposited them into fractures along with Ca-sulfate. The separation in B and Li would result due to differences in solubilities of the two elements and movement of the brine within VRR.

6.3 Possible alternative models

Well crystallized akageneite forms from the hydrolysis of Fe3+ in Cl-bearing solutions under acidic pH (Refait and Genin, 1997; Remazeilles and Refait, 2007; Zhao *et al*., 2012; Peretyazhko *et al*., 2016; 2018). Although the presence of jarosite and crystalline akaganeite indicate an acidic environment, mobilization of iron oxide in VRR could be suggestive of slightly alkaline and reducing fluids (L'Haridon *et al*., 2018; David *et al*., 2019).

Because of this, a significant possibility is that different generations of fluids could have had different pH values. Another possibility is that the boron found in the veins in and around VRR was not sourced locally. Boron has been observed over the 22 km of the rover's traverse (Gasda *et al.*, 2017). In that case, acidic ground water need not be invoked to leach the boron out of the phyllosilicates locally. Instead, this step could have occurred elsewhere, although at least mildly acidic fluids would aid in transporting the boron in solution to its precipitation sites within VRR. All of these possibilities are consistent with the extensive diagenetic activity for which there is evidence at VRR. To narrow down the above-mentioned possibilities, studies of terrestrial analogues as well as geochemical modeling for Martian aqueous solutions are required.

7 Conclusions

We report 33 new B detections in Ca-sulfate veins between sols 1548 and 2052. An increase of B detections are observed in Pahrump Hills, Hartmann's Valley, and Karasburg and in VRR (upper Pettegrove Point and Jura members). Boron detection frequency and its relative peak area show a weak inverse correlation with corrected Li concentration of the veins. This weak inverse correlation between B and Li is observed across the stratigraphy of Gale crater and may reflect the crystallization sequence from the diagenetic fluid as a result of end-stage dehydration of evaporative brines. Boron detection in the Murray members below VRR may be caused by remobilization of B from pre-existing borate evaporites into the Ca-sulfate rich late-stage veins by groundwater. The presence of pre-existing thin layers of borates is inferred based on evidence of elevated dehydration (e.g, desiccation cracks and chlorides) during emplacement the bedrock. The presence of minerals such as crystalline akageneite and jarosite in VRR indicate that at least one pulse of warm and acidic diagenetic fluid altered the VRR bedrock. We hypothesize that B and Li were drawn out of the bedrock due to dissolution of clay minerals by the diagenetic fluids rather than by remobilization of pre-existing evaporites in VRR. However, another possibility is that these materials originated from a more distant source. The weak inverse relationship of B with Li may result from the different solubilities of the elements, but more work is needed in the form of chemical modeling to fully tease out the relationship between these two elements in the groundwater. B is less soluble than Li and easily crystallizes out of the fluid as borates while Li remains in the fluid. The increase in Li in the late-stage diagenetic features may be a snapshot of the last vestiges of liquid diagenetic fluid flowing through rocks of VRR. This study of B and Li contributes to our understanding of the

diagenetic and dehydration history of VRR and how it may have influenced the geochemistry and habitability of Gale crater.

The geochemistry of late stage diagenetic features of Gale crater suggests that the subsurface environment was likely conducive for key prebiotic chemical reactions. Gale crater has undergone multiple episodes of groundwater activity throughout its history with changing Eh, pH, temperatures, and redox conditions (Nachon *et al.*, 2014; Lanza *et al.*, 2016; Hurowitz *et al.*, 2017; Frydenvang *et al*., 2019; L'Haridon *et al.*, 2019). This changing diagenetic environment could have, at some point in its history, been suitable for reactions between borates and organic molecules (Eigenbrode *et al.*, 2018; ten Kate, 2018) present in Gale crater. Li and B-rich brines in Andean salars show the presence of diverse microbial communities and indicate that hypersaline brines can be habitable (Haferburg *et al.,* 2017). If borate-organic molecules are detected in Gale crater, they would provide insights on the possibility of life on Mars and origin of life on Earth. Like other elements important for life (e.g., CHNOPS), searching for B on Mars is a high priority for understanding its past aqueous and habitable history.

Acknowledgments, Samples, and Data

This work was supported in Canada by McGill University, the NSERC Discovery program, and the Canadian Space Agency's support for Mars Science Laboratory Participating Scientists. Rover exploration, including ChemCam operations and this specific work, was supported in the US by the NASA Mars Exploration Program. ChemCam operations and science in France was supported by CNRS. D. Das thanks Dylan Paddock for help with data processing code. J. Frydenvang acknowledges the Carlsberg Foundation. The authors thank S. McLennan, K. Benison, and an anonymous reviewer for helpful comments on the manuscript. There are no real or perceived financial conflicts of interests for any author. There are also no other affiliations for any author that may be perceived as having a conflict of interest with respect to the results of this paper. All data supporting the conclusions can be found in supporting information data sets, in the Planetary Data System (PDS) repository (https://pds-geosciences.wustl.edu/missions/msl/chemcam.htm) and in a Zenodo data repository (Das, 2020: http://doi.org/10.5281/zenodo.3877377).

References

Abu-Sharar, T. M., Hani, N. B., & Al-Khader, S. (2014). Boron adsorption–desorption characteristics of irrigated soils in the Jordan Valley. *Geoderma Regional*, *2*, 50-59.

Achilles, C. (2018) *Analyses of Crystalline and X-Ray Amorphous Materials in Gale Crater Rocks and Soils*. https://doi.org/10.1016/j.geodrs.2014.09.007

Allen, R. D., & Kramer, H. (1957). Ginorite and sassolite from Death Valley, California. *American Mineralogist: Journal of Earth and Planetary Materials*, *42*(1-2), 56-61.

Averill, W. A., & Olson, D. L. (1978). A review of extractive processes for lithium from ores and brines. In *Lithium Needs and Resources* (pp. 305-313). Pergamon. https://doi.org/10.1016/B978-0-08-022733-7.50015-0

Banham, S. G., Gupta, S., Rubin, D. M., Watkins, J. A., Sumner, D. Y., Edgett, K. S., et al. (2018). Ancient Martian aeolian processes and palaeomorphology reconstructed from the Stimson formation on the lower slope of Aeolis Mons, Gale crater, Mars. *Sedimentology*, *65*(4), 993-1042. https://doi.org/10.1111/sed.12469

Becker, S., Thoma, I., Deutsch, A., Gehrke, T., Mayer, P., Zipse, H., et al. (2016). A high-yielding, strictly regioselective prebiotic purine nucleoside formation pathway. *Science*, *352*(6287), 833-836. https://doi.org/10.1126/science.aad2808

Becker, S., Feldmann, J., Wiedemann, S., Okamura, H., Schneider, C., Iwan, K., et al. (2019). Unified prebiotically plausible synthesis of pyrimidine and purine RNA ribonucleotides. *Science*, *366*(6461), 76-82. https://doi.org/10.1126/science.aax2747

Benison, K. C. (2013). Acid saline fluid inclusions: examples from modern and Permian extreme lake systems. *Geofluids*, *13*(4), 579-593. https://doi.org/10.1111/gfl.12053

Biggar, J. W., & Fireman, M. (1960). Boron Adsorption and Release by Soils 1. *Soil Science Society of America Journal*, *24*(2), 115-120. https://doi.org/10.2136/sssaj1960.03615995002400020015x

Bingham, F., Page, A. L., Coleman, N. T., & Flach, K. (1971). Boron Adsorption Characteristics of Selected Amorphous Soils from Mexico and Hawaii 1. *Soil Science Society of America Journal*, *35*(4), 546-550. https://doi.org/10.2136/sssaj1971.03615995003500040021x

Birsoy, R., & Özbaş, Ü. (2012). Activity diagrams of borates: implications on common deposits. *Carbonates and Evaporites*, *27*(1), 71-85. https://doi.org/10.1007/s13146-012-0085-6

Blasdale, W. C., & Slansky, C. M. (1939). The solubility curves of boric acid and the borates of sodium. *Journal of the American Chemical Society*, *61*(4), 917-920. https://doi.org/10.1021/ja01873a043

Bodnar, R. J. (1999). *Fluid Inclusions in ALH84001 and Other Martian Meteorites: Evidence for Volatiles on Mars.* Abstract number 1222. Presented at the 30th Lunar and Planetary Science Conference, Houston, TX.

Bridges, J. C., Cousin, A., Sautter, V., Rapin, W., Schwenzer, S. P., Bedford, C., et al. (2019). *Askival: A Silicified Feldspathic Cumulate Sample in Gale Crater.* Abstract number 2345. Presented at the 50th Lunar and Planetary Science Conference, Houston, TX.

Bristow, T. F., Rampe, E. B., Achilles, C. N., Blake, D. F., Chipera, S. J., Craig, P., et al. (2018). Clay mineral diversity and abundance in sedimentary rocks of Gale crater, Mars. *Science Advances*, *4*(6), eaar3330. https://doi.org/10.1126/sciadv.aar3330

Burst, J. F. (1957). Postdiagenetic clay mineral environmental relationships in the Gulf Coast Eocene. *Clays and Clay Minerals*, *6*(1), 327-341. https://doi.org/10.1346/CCMN.1957.0060124

Casas, E., & Lowenstein, T. K. (1989). Diagenesis of saline pan halite; comparison of petrographic features of modern, Quaternary and Permian halites. *Journal of Sedimentary Research*, *59*(5), 724-739. https://doi.org/10.1306/212F905C-2B24-11D7-8648000102C1865D

Christ, C. L., Truesdell, A. H., & Erd, R. C. (1967). Borate mineral assemblages in the system Na2O- CaO-MgO-B2O3-H2O. *Geochimica et Cosmochimica Acta*, *31*(3), 313-337. https://doi.org/10.1016/0016-7037(67)90045-2

Clegg, S. M., Sklute, E., Dyar, M. D., Barefield, J. E., & Wiens, R. C. (2009). Multivariate analysis of remote laser-induced breakdown spectroscopy spectra using partial least squares, principal component analysis, and related techniques. *Spectrochimica Acta Part B: Atomic Spectroscopy*, *64*(1), 79-88. https://doi.org/10.1016/j.sab.2008.10.045

Clegg, S. M., Wiens, R. C., Anderson, R., Forni, O., Frydenvang, J., Lasue, J., et al. (2017). Recalibration of the Mars Science Laboratory ChemCam instrument with an expanded geochemical database. *Spectrochimica Acta Part B: Atomic Spectroscopy*, *129*, 64-85. https://doi.org/10.1016/j.sab.2016.12.003.

Cloutis, E., Berg, B., Mann, P., & Applin, D. (2016). Reflectance spectroscopy of low atomic weight and Na-rich minerals: Borates, hydroxides, nitrates, nitrites, and peroxides. *Icarus*, *264*, 20-36. https://doi.org/10.1016/j.icarus.2015.08.026.

Correns, C. W. (2003). Fluid inclusions with gas bubbles as geothermometers. *International Journal of Earth Sciences*, *91*(0), s123–s133. https://doi.org/10.1007/s00531-002-0273-z

Couch, E. L., & Grim, R. E. (1968). Boron fixation by illites. *Clays and Clay Minerals*, *16*(3), 249-256. https://doi.org/10.1346/CCMN.1968.0160307

Csetenyi, L. J., & Glasser, F. P. (1992). Borate substituted ettringites. *MRS Online Proceedings Library Archive*, *294*. https://doi.org/10.1557/PROC-294-273

Dalton, G. R., Lee, A. Y., & Young, S. L. (2016). *IUPAC/NIST Solubility Database* (No. IUPAC/NIST Solubility Database).

Das, D. (2020). ChemCam data and corrected Li data [Data set]. Zenodo. http://doi.org/10.5281/zenodo.3877377

David, G., Cousin, A., Forni, O., Meslin, P. Y., Mangold, N., L'Haridon, J., et al. (2019). *Hematite Mineral Grains Observed by ChemCam Across the Vera Rubin Ridge Sedimentary Rocks at Gale Crater, Mars.* Presented at the Ninth International Conference on Mars, LPI Contributions, Pasadena, CA.

Eberl, D., & Hower, J. (1976). Kinetics of illite formation. *Geological Society of America Bulletin*, *87*(9), 1326-1330. https://doi.org/10.1130/0016-7606(1976)87<1326:KOIF>2.0.CO;2

Edgar, L. A., Fraeman, A. A., Gupta, S., Fedo, C. M., Grotzinger, J. P., Stack, K. M., et al. (2018). *Sedimentology and Stratigraphy Observed at Vera Rubin Ridge by the Mars Science Laboratory Curiosity Rover.* Abstract number 1704. Presented at the 49th Lunar and Planetary Science Conference, Houston, TX.

Edgett, K. S., Yingst, R. A., Ravine, M. A., Caplinger, M. A., Maki, J. N., Ghaemi, F. T., et al. (2012). Curiosity's Mars hand lens imager (MAHLI) investigation. *Space Science Reviews*, *170*(1-4), 259-317. https://doi.org/10.1007/s11214-012-9910-4

Ehlmann, B. L., Swayze, G. A., Milliken, R. E., Mustard, J. F., Clark, R. N., Murchie, S. L., et al. (2016). Discovery of alunite in Cross crater, Terra Sirenum, Mars: Evidence for acidic, sulfurous waters. *American Mineralogist*, *101*(7), 1527-1542. https://doi.org/10.2138/am-2016-5574

Eigenbrode, J. L., Summons, R. E., Steele, A., Freissinet, C., Millan, M., Navarro-González, R., et al. (2018). Organic matter preserved in 3-billion-year-old mudstones at Gale crater, Mars. *Science*, *360*(6393), 1096-1101. https://doi.org/10.1126/science.aas9185

Evans, C. M., & Sparks, D. L. (1983). On the chemistry and mineralogy of boron in pure and in mixed systems: A review. *Communications in Soil Science and Plant Analysis*, *14*(9), 827-846. https://doi.org/10.1080/00103628309367412

Fan, Q., Ma, Y., Cheng, H., Wei, H., Yuan, Q., Qin, Z., & Shan, F. (2015). Boron occurrence in halite and boron isotope geochemistry of halite in the Qarhan Salt Lake, western China. *Sedimentary Geology*, *322*, 34-42. https://doi.org/10.1016/j.sedgeo.2015.03.012

Fedo, C. M., Grotzinger, J. P., Gupta, S., Fraeman, A., Edgar, L., Edgett, K., et al. (2018). *Sedimentology and Stratigraphy of the Murray Formation, Gale Crater, Mars.* Abstract number 2078. Presented at the 49th Lunar and Planetary Science Conference, Houston, TX.

Fedo, C. M., Grotzinger, J. P., Gupta, S., Stein, N. T., Watkins, J., Banham, S., et al. (2017). *Facies analysis and basin architecture of the upper part of the Murray formation, Gale Crater, Mars*. Abstract number 1689. Presented at the 48th Lunar and Planetary Science Conference, Houston, TX.

Forni, O., Vaniman, D. T., Le Deit, L., Clegg, S. M., Lanza, N. L., Lasue, J., et al. (2015). *Fluorine and lithium at the Kimberley outcrop, Gale Crater*. Abstract number 1989. Presented at the 46th Lunar and Planetary Science

Conference, Houston, TX.

Forni, O., Meslin, P. Y., Cousin, A., Clegg, S. M., Mangold, N., Le Deit, L., et al. (2019). *Fluorine on Mars: Seven Years of Detection with ChemCam On-Board MSL*. Abstract number 6095. Presented at the Ninth International Conference on Mars, LPI Contributions, Pasadena, CA..

Forni, O., Meslin, P. Y., L'Haridon, J., Rapin, W., Nachon, M., Newsom, H., et al. (2017). *Detection of Fluorine-Rich Phases, Phosphates, and Halite in the Stimson-Murray Units, Gale Crater, Mars*. Abstract number 1838. Presented at the 48th Lunar and Planetary Science Conference, Houston, TX.

Fraeman, A. A., Catalano, J. G., Edgar, L. A., Fischer, W. W., Grotzinger, J. P., L'Haridon, J., et al. (2019). *Vera Rubin Ridge and Iron Oxide Bearing Sedimentary Rocks on Mars: The Integrated View from Curiosity and Orbital Data.* Abstract number 6237. Presented at the Ninth International Conference on Mars, LPI Contributions, Pasadena, CA.

Fraeman, A. A., Arvidson, R. E., Catalano, J. G., Grotzinger, J. P., Morris, R. V., Murchie, S. L, et al. (2013). A Hematite-Bearing Layer in Gale Crater, Mars: Mapping and Implications for Past Aqueous Conditions. *Geology*, *41*(10), 1103-1106. https://doi.org/10.1130/G34613.1

Fraeman, A. A., Edgar, L. A., Grotzinger, J. P., Vasavada, A. R., Johnson, J. R., Wellington, D. F., et al. (2018). *Curiosity's Investigation at Vera Rubin Ridge.* Presented at the 49th Lunar and Planetary Science Conference, Houston, TX.

Frederickson, A. F., & Reynolds, R. C., Jr. (1960). Geochemical Method for Determining Paleosalinity. *Clays and Clay Minerals* (pp. 203-213). Pergamon. https://doi.org/10.1016/B978-0-08-009351-2.50023-4

Frydenvang, J., Mangold, N., Wiens, R. C., Fraeman, A. A., Edgar, L. A., Fedo, C. M., et al. (2019). *The chemostratigraphy of the lacustrine Murray formation in Gale crater, Mars, and evidence for large-scale diagenesis in Vera Rubin ridge bedrock as implied by ChemCam observations.* Abstract number 6334. Presented at the Ninth International Conference on Mars, LPI Contributions, Pasadena, CA.

Furukawa, Y., Chikaraishi, Y., Ohkouchi, N., Ogawa, N. O., Glavin, D. P., Dworkin, J. P., et al. (2019). Extraterrestrial ribose and other sugars in primitive meteorites. *Proceedings of the National Academy of Sciences, 116(49),* 24440-24445. https://doi.org/10.1073/pnas.1907169116

Furukawa, Y., Horiuchi, M., & Kakegawa, T. (2013). Selective stabilization of ribose by borate. *Origins of Life and Evolution of Biospheres, 43*(4-5), 353-361. https://doi.org/10.1007/s11084-013-9350-5

Furukawa, Y., & Kakegawa, T. (2017). Borate and the Origin of RNA: A Model for the Precursors to Life. *Elements, 13*(4), 261-265. https://doi.org/10.2138/gselements.13.4.261

Garrett, D. E. (1998). *Borates: Handbook of deposits, processing, properties, and use*. Elsevier, 482-483.

Gasda, P. J., Haldeman, E. B., Wiens, R. C., Rapin, W., Bristow, T. F., Bridges, J. C., et al. (2017). In situ detection of boron by ChemCam on Mars. *Geophysical Research Letters*, *44*(17), 8739-8748. https://doi.org/10.1002/2017GL074480.

Gast, R. G., & Klobe, W. D. (1971). Sodium-lithium exchange equilibria on vermiculite at 25 and 50 C. *Clays and Clay Minerals*, *19*(5), 311-319.

Glotch, T. D., Bandfield, J. L., Tornabene, L. L., Jensen, H. B., & Seelos, F. P. (2010). Distribution and formation of chlorides and phyllosilicates in Terra Sirenum, Mars. *Geophysical Research Letters, 37*(16). https://doi.org/10.1029/2010GL044557

Goldberg, S. (1997). Reactions of boron with soils. *Plant and Soil*, *193*(1-2), 35-48. https://doi.org/10.1023/A:1004203723343

Goldberg, S., Forster, H. S., & Heick, E. L. (1993). Temperature effects on boron adsorption by reference minerals and soils. *Soil Science*, *156*(5), 316-321. https://doi.org/10.1097/00010694-199311000-00004

Goldberg, S., Suarez, D. L., & Shouse, P. J. (2008). Influence of soil solution salinity on boron adsorption by soils. *Soil Science*, *173*(6), 368-374.

Goldstein, R. H., & Samson, I. (2003). Petrographic analysis of fluid inclusions. *Fluid Inclusions: Analysis and Interpretation, 32*, 9-53.

Greene-Kelly, R. (1955). Lithium absorption by kaolin minerals. *The Journal of Physical Chemistry*, *59*(11), 1151-1152. https://doi.org/10.1021/j150533a009

Grew, E. S. (2017). Boron: from cosmic scarcity to 300 minerals. *Elements*, *13*(4), 225-229. https://doi.org/10.2138/gselements.13.4.225

Grew, E. S., Bada, J. L., & Hazen, R. M. (2011). Borate minerals and origin of the RNA world. *Origins of Life and Evolution of Biospheres*, *41*(4), 307-316. https://doi.org/10.1007/s11084-010-9233-y

Grotzinger, J. P., Sumner, D. Y., Kah, L. C., Stack, K., Gupta, S., Edgar, L., et al. (2014). A habitable fluvio-lacustrine environment at Yellowknife Bay, Gale Crater, Mars. *Science*, *343*(6169), 1242777. https://doi.org/10.1126/science.1242777

Grotzinger, J. P., Gupta, S., Malin, M. C., Rubin, D. M., Schieber, J., Siebach, K., et al. (2015). Deposition, exhumation, and paleoclimate of an ancient lake deposit, Gale crater, Mars. *Science*, *350*(6257), aac7575. https://doi.org/10.1126/science.aac7575

Grotzinger, J. P., & Milliken, R. E. (2012). The sedimentary rock record of Mars: Distribution, origins, and global stratigraphy. *Sedimentary Geology of Mars*, *102*, 1-48.

Gwizd, S., Fedo, C., Grotzinger, J., Edgett, K., Rivera-Hernandez, F., & Stein, N. (2018). *Depositional History of the Hartmann's Valley Member, Murray Formation, Gale Crater, Mars.* Abstract number 2150. Presented at the 49th Lunar and Planetary Science Conference, Houston, TX.

Haber, J. T., Horgan, B., Fraeman, A. A., Johnson, J. R., Wellington, D., Bell, J. F., et al. (2019). *Mineralogy of a Possible Ancient Lakeshore in Gale Crater, Mars, from Mastcam Multispectral Images*. Abstract number 6229. Presented at the Ninth International Conference on Mars, LPI Contributions, Pasadena, CA.

Haferburg, G., Gröning, J. A., Schmidt, N., Kummer, N. A., Erquicia, J. C., & Schlömann, M. (2017). Microbial diversity of the hypersaline and lithium-rich Salar de Uyuni, Bolivia. *Microbiological Research*, *199*, 19-28. https://doi.org/10.1016/j.micres.2017.02.007

Hall, B. E. (1977). *U.S. Patent No. 4,056,146*. Washington, DC: U.S. Patent and Trademark Office.

Hamzaoui, A. H., M'nif, A., Hammi, H., & Rokbani, R. (2003). Contribution to the lithium recovery from brine. *Desalination*, *158*(1-3), 221-224. https://doi.org/10.1016/S0011-9164(03)00455-7

Harder, H. A. (1970). Boron content of sediments as a tool in facies analysis. *Sedimentary Ggeology*, *4*(1-2), 153-175. https://doi.org/10.1016/0037-0738(70)90009-6

Hardie, L. A. (1967). The gypsum—anhydrite equilibrium at one atmosphere pressure. *American Mineralogist*, *52*(1-2), 171-200.

Helvaci, C. (1977). *Geology, mineralogy and geochemistry of the borate deposits and associated rocks at the Emet Valley, Turkey* (Doctoral dissertation, University of Nottingham).

Helvaci, C., & Alaca, O. (1991). Geology and Mineralogy of the Bigadiç Borate Deposıts and Vicinity. *Bulletin of the Mineral Research and Exploration*, 113(113), 31-63.

Helvacı, C., Stamatakis, M. G., Zagouroglou, C., & Kanaris, J. (1993). Borate minerals and related authigenic silicates in northeastern Mediterranean late Miocene continental basins. *Exploration and Mining Geology*, *2*(2), 171-178.

Helvaci, C., & Orti, F. (1998). Sedimentology and diagenesis of Miocene colemanite-ulexite deposits (western Anatolia, Turkey). *Journal of Sedimentary Research*, *68*(5), 1021-1033.

Helvaci, C., & Ortí, F. (2004). Zoning in the Kirka borate deposit, western Turkey: primary evaporitic fractionation or diagenetic modifications? *The Canadian Mineralogist*, *42*(4), 1179-1204. https://doi.org/10.2113/gscanmin.42.4.1179

Helvaci, C., & Palmer, M. R. (2017). Origin and Distribution of Evaporite Borates: The Primary Economic Sources of Boron. *Elements*, *13*(4), 249-254. https://doi.org/10.2138/gselements.13.4.249

Hemming, N. G., Reeder, R. J., & Hanson, G. N. (1995). Mineral-fluid partitioning and isotopic fractionation of boron in synthetic calcium carbonate. *Geochimica et Cosmochimica Acta*, *59*(2), 371-379. https://doi.org/10.1016/0016-7037(95)00288-B

Heydari, E., Parker, T. J., Calef III, F. J., Schroeder, J. F., Van Beek, J., Rowland, S. K., & Fairen, A. G. (2018). *Characteristics and the Origin of the Vera Rubin Ridge, Gale Crater, Mars.* Abstract number 1817. Presented at the 49th Lunar and Planetary Science Conference, Houston, TX.

Hilgers, C., & Urai, J. L. (2002). Microstructural observations on natural syntectonic fibrous veins: implications for the growth process. *Tectonophysics*, *352*(3-4), 257-274. https://doi.org/10.1016/S0040-1951(02)00185-3.

Hingston, F. J. (1964). Reactions between boron and clays. *Soil Research*, *2*(1), 83-95. https://doi.org/10.1071/SR9640083

Horgan, B., Fraeman, A., Johnson, J. R., Thompson, L., Jacob, S., Bell, J. F., & Grotzinger, J. (2019). *Redox Conditions During Diagenesis in the Vera Rubin Ridge, Gale Crater, Mars, from Mastcam Multispectral Images*. Abstract number 1424. Presented at the 50th Lunar and Planetary Science Conference, Houston, TX.

Huang, W. H., & Keller, W. D. (1971). Dissolution of clay minerals in dilute organic acids at room temperature. *American Mineralogist: Journal of Earth and Planetary Materials*, *56*(5-6), 1082-1095.

Hud, N. V., & Fialho, D. M. (2019). RNA nucleosides built in one prebiotic pot. *Science*, *366*(6461), 32-33. https://doi.org/10.1126/science.aaz1130

Hunt, C. B. (1966). *Hydrologic Basin, Death Valley, California* (No. 494). US Government Printing Office. https://doi.org/10.3133/pp494B

Hurowitz, J. A., Grotzinger, J. P., Fischer, W. W., McLennan, S. M., Milliken, R. E., Stein, N., et al (2017). Redox stratification of an ancient lake in Gale crater, Mars. *Science*, *356*(6341), eaah6849. https://doi.org/10.1126/science.aah6849

Inan, K. (1973). Mineralogy, Chemistry and Origin of Kirka Borate Deposit, Eskishehir Province, Turkey. *Serial Issue in Instit. Ming Metallurgy Bull.*, 82(801), 114-123

Johnson, J. R., Bell, J. F., Lemmon, M., & Pinet, P. (2019). *Mastcam Visible/Near-Infrared Spectrophotometric Observations of the Red Hills Region of Vera Rubin Ridge*. Abstract number 1313. Presented at the 50th Lunar and Planetary Science Conference.

Kah, L. C., Stack, K. M., Eigenbrode, J. L., Yingst, R. A., & Edgett, K. S. (2018). Syndepositional precipitation of calcium sulfate in Gale Crater, Mars. *Terra Nova*, *30*(6), 431-439. https://doi.org/10.1111/ter.12359

Karahan, S. *et al.* (2006) 'Removal of boron from aqueous solution by clays and modified clays', *Journal of Colloid and Interface Science*, 293(1), pp. 36–42. doi: 10.1016/j.jcis.2005.06.048.

ten Kate, I. L. (2018). Organic molecules on Mars. *Science*, *360*(6393), 1068-1069. https://doi.org/10.1126/science.aat2662

Keren, R., & O'connor, G. A. (1982). Effect of exchangeable ions and ionic strength on boron adsorption by montmorillonite and illite. *Clays and Clay minerals*, *30*(5), 341-346. https://doi.org/10.1346/CCMN.1982.0300504

Keren, R., & Mezuman, U. (1981). Boron adsorption by clay minerals using a phenomenological equation. *Clays and Clay Minerals*, *29*(3), 198-204. https://doi.org/10.1346/CCMN.1981.0290305

Keren, R., Gast, R. G., & Bar-Yosef, B. (1981). pH-Dependent Boron Adsorption by Na-Montmorillonite 1. *Soil Science Society of America Journal*, *45*(1), 45-48. https://doi.org/10.2136/sssaj1981.03615995004500010010x

Kim, H. J., Ricardo, A., Illangkoon, H. I., Kim, M. J., Carrigan, M. A., Frye, F., & Benner, S. A. (2011). Synthesis of carbohydrates in mineral-guided prebiotic cycles. *Journal of the American Chemical Society*, *133*(24), 9457-9468. https://doi.org/10.1021/ja201769f

Kistler, R. B., & Helvaci, C. (1994). Boron and Borates. *Industrial minerals and rocks, Society of Mining Engineers, 6(5),* 171-186.

Kitano, Y., Okumura, M., & Idogaki, M. (1978). Coprecipitation of borate-boron with calcium carbonate. *Geochemical Journal*, *12*(3), 183-189. https://doi.org/10.2343/geochemj.12.183

Kronyak, R. E., Kah, L. C., Edgett, K. S., VanBommel, S. J., Thompson, L. M., Wiens, R. C., et al. (2019). Mineral-filled fractures as indicators of multigenerational fluid flow in the Pahrump Hills member of the Murray formation, Gale crater, Mars. *Earth and Space Science*, *6*(2), 238-265. https://doi.org/10.1029/2018EA000482

Krüger, Y., García-Ruiz, J. M., Canals, À., Marti, D., Frenz, M., & Van Driessche, A. E. (2013). Determining gypsum growth temperatures using monophase fluid inclusions—Application to the giant gypsum crystals of Naica, Mexico. *Geology*, *41*(2), 119-122. https://doi.org/10.1130/G33581.1

L'Haridon, J., Mangold, N., Meslin, P. Y., Johnson, J. R., Rapin, W., Forni, O., et al. (2018). Chemical variability in mineralized veins observed by ChemCam on the lower slopes of Mount Sharp in Gale crater, Mars. *Icarus*, *311*, 69-86. https://doi.org/10.1016/j.icarus.2018.01.028

L'Haridon, J., Mangold, N., Wiens, R. C., Cousin, A., David, G., Johnson, J. R., et al. (2019). *Iron-Rich Diagenetic Features Analysed In the Murray Formation at Gale Crater, Mars, Using Chemcam Onboard the Curiosity Rover.* Abstract number 6079. Presented at the Ninth International Conference on Mars, LPI Contributions, Pasadena, CA.

Lanza, N. L., Wiens, R. C., Arvidson, R. E., Clark, B. C., Fischer, W. W., Gellert, R., et al. (2016). Oxidation of manganese in an ancient aquifer, Kimberley formation, Gale crater, Mars. *Geophysical Research Letters*, *43*(14), 7398-7407. https://doi.org/10.1002/2016GL069109

Larralde, R., Robertson, M. P., & Miller, S. L. (1995). Rates of decomposition of ribose and other sugars: implications for chemical evolution. *Proceedings of the National Academy of Sciences*, *92*(18), 8158-8160. https://doi.org/10.1073/pnas.92.18.8158

Lerman, A. (1966). Boron in clays and estimation of paleosalinities. *Sedimentology*, *6*(4), 267-286. https://doi.org/10.1111/j.1365-3091.1966.tb01895.x

Li, Q., Fan, Q., Wang, J., Qin, Z., Zhang, X., Wei, H., & Shan, F. (2019). Hydrochemistry, Distribution and Formation of Lithium-Rich Brines in Salt Lakes on the Qinghai-Tibetan Plateau. *Minerals*, *9*(9), 528. https://doi.org/10.3390/min9090528

Lowenstein, T. K., Li, J., & Brown, C. B. (1998). Paleotemperatures from fluid inclusions in halite: method verification and a 100,000-year paleotemperature record, Death Valley, CA. *Chemical Geology*, *150*(3-4), 223-245. https://doi.org/10.1016/S0009-2541(98)00061-8

Malin, M. C., Caplinger, M. A., Edgett, K. S., Ghaemi, F. T., Ravine, M. A., Schaffner, J. A., et al. (2010). *The Mars Science Laboratory (MSL) mast-mounted cameras (Mastcams) flight instruments.* Abstract number 1123. Presented at the 41st Lunar and Planetary Science Conference, Houston, TX.

Mangold, N., Schmidt, M. E., Fisk, M. R., Forni, O., McLennan, S. M., Ming, D. W., et al. (2017). Classification scheme for sedimentary and igneous rocks in Gale crater, Mars. *Icarus*, *284*, 1-17. https://doi.org/10.1016/j.icarus.2016.11.005

Mangold, N., Dehouck, E., Fedo, C., Forni, O., Achilles, C., Bristow, T., et al. (2019). Chemical alteration of fine-grained sedimentary rocks at Gale crater. *Icarus*, *321*, 619-631. https://doi.org/10.1016/j.icarus.2018.11.004

Marion, G. M., Mikhail V. Mironenko, & Morien W. Roberts (2010). "FREZCHEM: A geochemical model for cold aqueous solutions." *Computers & Geosciences*, 36.1, 10-15. https://doi.org/10.1016/j.cageo.2009.06.004

Martin, P. E., Farley K. A., Baker, M. B., Malespin, C. A., Schwenzer, S. P., Cohen, B. A., et al. (2017) "A two-step K-Ar experiment on Mars: Dating the diagenetic formation of jarosite from Amazonian groundwaters." *Journal of Geophysical Research: Planets 122(1),* 2803-2818. https://doi.org/10.1002/2017JE005445

Maurice, S., Wiens, R. C., Saccoccio, M., Barraclough, B., Gasnault, O., Forni, O., et al. (2012). The ChemCam instrument suite on the Mars Science Laboratory (MSL) rover: Science objectives and mast unit description. *Space Science Reviews*, *170*(1-4), 95-166. https://doi.org/10.1007/s11214-012-9912-2

Mavromatis, V., Montouillout, V., Noireaux, J., Gaillardet, J., & Schott, J. (2015). Characterization of boron incorporation and speciation in calcite and aragonite from co-precipitation experiments under controlled pH, temperature and precipitation rate. *Geochimica et Cosmochimica Acta*, *150*, 299-313. https://doi.org/10.1016/j.gca.2014.10.024

McLennan, S. M., Anderson, R. B., Bell, J. F., Bridges, J. C., Calef, F., Campbell, J. L., et al. (2014). Elemental geochemistry of sedimentary rocks at Yellowknife Bay, Gale crater, Mars. *Science*, *343*(6169), 1244734. http://doi.org/10.1126/science.1244734

Mianping, Z., Zhao Y., & Liu J. (2000) "Palaeoclimatic indicators of China's Quaternary saline lake sediments and hydrochemistry." *Acta Geologica Sinica-English Edition 74(2)*: 259-265. https://doi.org/10.1111/j.1755-6724.2000.tb00459.x

Ming, D. W., Archer, P. D., Glavin, D. P., Eigenbrode, J. L., Franz, H. B., Sutter, B., et al. (2014). Volatile and organic compositions of sedimentary rocks in Yellowknife Bay, Gale Crater, Mars. *Science*, *343*(6169), 1245267. https://doi.org/10.1126/science.1245267

Miranda-Gasca, M. A., Gomez-Caballero, J. A., & Eastoe, C. J. (1998). Borate deposits of northern Sonora, Mexico; stratigraphy, tectonics, stable isotopes, and fluid inclusions. *Economic Geology*, *93*(4), 510-523. https://doi.org/10.2113/gsecongeo.93.4.510

Morris, R. V., Bristow, T. F., Rampe, E. B., Yen, A. S., Vaniman, D. T., Tu, V., et al. (2019). *Mineralogy and Formation Processes for the Vera Rubin Ridge at Gale Crater, Mars from CheMin XRD Analyses.* Abstract number 1127. Presented at the 50th *Lunar and Planetary Science Conference*, Houston, TX.

Munk, L. A., Boutt, D. F., Hynek, S. A., & Moran, B. J., (2018). Hydrogeochemical fluxes and processes contributing to the formation of lithium-enriched brines in a hyper-arid continental basin. *Chemical Geology*, *493*, 37-57. https://doi.org/10.1016/j.chemgeo.2018.05.013

Le Mouélic, S., Gasnault, O., Herkenhoff, K. E., Bridges, N. T., Langevin, Y., Mangold, N., et al. (2015). The ChemCam Remote Micro-Imager at Gale crater: Review of the first year of operations on Mars. *Icarus*, *249*, 93-107. https://doi.org/10.1016/j.icarus.2014.05.030

Nachon, M., Clegg, S. M., Mangold, N., Schröder, S., Kah, L. C., Dromart, G., et al. (2014). Calcium sulfate veins characterized by ChemCam/Curiosity at Gale crater, Mars. *Journal of Geophysical Research: Planets*, *119*(9), 1991-2016. https://doi.org/10.1002/2013JE004588

Nachon, M., Mangold, N., Forni, O., Kah, L. C., Cousin, A., Wiens, R. C., et al. (2017). Chemistry of diagenetic features analyzed by ChemCam at Pahrump Hills, Gale crater, Mars. *Icarus*, *281*, 121-136. https://doi.org/10.1016/j.icarus.2016.08.026

Nir, S., Hirsch, D., Navrot, J., & Banin. A., (1986) "Specific adsorption of lithium, sodium, potassium, and strontium to montmorillonite: observations and predictions." *Soil Science Society of America Journal* 50, no. 1, 40-45. https://doi.org/10.2136/sssaj1986.03615995005000010008x

Palmer, M. R., Spivack, A. J., & Edmond, J. M. (1987). Temperature and pH controls over isotopic fractionation during adsorption of boron on marine clay. *Geochimica et Cosmochimica Acta*, *51*(9), 2319-2323. https://doi.org/10.1016/0016-7037(87)90285-7

Palmer, M. R., & Helvaci, C. (1997). The boron isotope geochemistry of the Neogene borate deposits of western Turkey. *Geochimica et Cosmochimica Acta*, *61*(15), 3161-3169. https://doi.org/10.1016/S0016-7037(97)00135-X

Payré, V., Fabre, C., Cousin, A., Sautter, V., Wiens, R. C., Forni, O., et al. (2017). Alkali trace elements in Gale crater, Mars, with ChemCam: Calibration update and geological implications. *Journal of Geophysical Research: Planets*, *122*(3), 650-679. https://doi.org/10.1002/2016JE005201

Peretyazhko, T. S., Fox, A., Sutter, B., Niles, P. B., Adams, M., Morris, R. V., and Ming, D. W. (2016). Synthesis of akaganeite in the presence of sulfate: Implications for akaganeite formation in Yellowknife Bay, Gale crater, Mars. *Geochimica et Cosmochimica Acta*, *188*, 284-296, http://dx.doi.org/10.1016/j.gca.2016.06.002.

Peretyazhko, T. S., Ming, D. W., Rampe, E. B., Morris, R. V., and Agresti, D. G. (2018). Effect of solution pH and chloride concentration on akaganeite precipitation: Implications for akaganeite formation on Mars. *Journal of Geophysical Research: Planets*, *123*, 2211-2222, http://dx.doi.org/10.1029/2018JE005630.

Perry, E. A. (1972). Diagenesis and the validity of the boron paleosalinity technique. *American Journal of Science*, *272*(2), 150-160. https://doi.org/10.2475/ajs.272.2.150

Powner, M. W., Gerland, B., & Sutherland, J. D. (2009). Synthesis of activated pyrimidine ribonucleotides in prebiotically plausible conditions. *Nature*, *459*(7244), 239. https://doi.org/10.1038/nature08013

Rampe, E. B., Bristow, T. F., Blake, D. F., Morris, R. V., Ming, D. W., Achilles, C. N., et al. (2019). *The Mineralogical Record of Ancient Fluvio-Lacustrine Environments in Gale Crater as Measured by the MSL CheMin Instrument*. Abstract number 6054. Presented at the Ninth International Conference on Mars, LPI Contributions, Pasadena, CA.

Rapin, W., Ehlmann, B. L., Dromart, G., Schieber, J., Thomas, N. H., Fischer, W. W., et al. (2019). An interval of high salinity in ancient Gale crater lake on Mars. *Nature Geoscience*, *12*(11), 889-895. https://doi.org/10.1038/s41561-019-0458-8

Rapin, W., Meslin, P. Y., Maurice, S., Vaniman, D., Nachon, M., Mangold, N., et al., (2016). Hydration state of calcium sulfates in Gale crater, Mars: Identification of bassanite veins. *Earth and Planetary Science Letters*, *452*, 197-205. https://doi.org/10.1016/j.epsl.2016.07.045

Refait, P., and Génin, J. -M. R. (1997). The mechanisms of oxidation of ferrous hydroxychloride β -$Fe_2(OH)_3Cl$ in aqueous solution: The formation of akaganeite vs. goethite. *Corrosion Science*, *39*(3), 539-553, http://dx.doi.org/10.1016/S0010-938X(97)86012-1

Rémazeilles, C., and Refait, P. (2007). On the formation of β -FeOOH (akaganeite) in chloride-containing environments. *Corrosion Science*, *49*(2), 844-857, http://dx.doi.org/10.1016/j.corsci.2006.06.003.

Risacher, F.& Fritz, B. (2009) "Origin of salts and brine evolution of Bolivian and Chilean salars." *Aquatic Geochemistry 15(1-2)*, 123-157. https://doi.org/10.1007/s10498-008-9056-x

Risacher, F., & Fritz, B. (1991). Quaternary geochemical evolution of the salars of Uyuni and Coipasa, Central Altiplano, Bolivia. *Chemical Geology*, *90*(3-4), 211-231.

Rivera-Hernández, F., Sumner, D. Y., Mangold, N., Stack, K. M., Forni, O., Newsom, H., et al. (2019). Using ChemCam LIBS data to constrain grain size in rocks on Mars: Proof of concept and application to rocks at Yellowknife Bay and Pahrump Hills, Gale crater. *Icarus*, *321*, 82-98. https://doi.org/10.1016/j.icarus.2018.10.023

Ruiz-Mirazo, K., Briones, C., & de la Escosura, A. (2013). Prebiotic systems chemistry: new perspectives for the origins of life. *Chemical Reviews*, *114*(1), 285-366. https://doi.org/10.1021/cr2004844

Sansonetti, J. E., & Martin, W. C. (2005). Handbook of basic atomic spectroscopic data. *Journal of Physical and Chemical Reference Data*, *34*(4), 1559-2259. https://doi.org/10.1063/1.1800011

Schwenzer, S. P., Abramov, O., Allen, C. C., Clifford, S. M., Cockell, C. S., Filiberto, J., Treiman, A. H., et al. (2012). Puncturing Mars: How impact craters interact with the Martian cryosphere. *Earth and Planetary Science Letters*, *335*, 9-17. https://doi.org/10.1016/j.epsl.2012.04.031

Schwenzer, S. P., Bridges, J. C., Wiens, R. C., Conrad, P. G., Kelley, S. P., Leveille, R., et al. (2016). Fluids during diagenesis and sulfate vein formation in sediments at Gale crater, Mars. *Meteoritics & Planetary Science*, *51*(11), 2175-2202. https://doi.org/10.1111/maps.12668

Seryotkin, Y. V., Sokol, E. V., Kokh, S. N., & Murashko, M. N. (2018). Natural Cr 3^{+}-rich ettringite: occurrence, properties, and crystal structure. *Physics and Chemistry of Minerals*, *45*(3), 279-292. https://doi.org/10.1007/s00269-017-0917-y

Seyfried, W. E., Janecky, D. R., & Mottl, M. J. (1984) "Alteration of the oceanic crust: implications for geochemical cycles of lithium and boron." *Geochimica et Cosmochimica Acta* 48(3), 557-569. https://doi.org/10.1016/0016-7037(84)90284-9

Siebach, K. L., Fedo, C. M., Edgar, L. E., Edgett, K., Grotzinger, J. P., Fraeman, A. A., et al. (2019, March). *Overview of Gale Crater Stratigraphy and Sedimentology from 6 Years of Roving with Mars Science Laboratory.* Abstract number 1479. Presented at the 50th *Lunar and Planetary Science Conference*, Houston, TX.

Siefke, J. W. (1991). The Boron open pit mine at the Kramer borate deposit. *The Diversity of Mineral and Energy Resources of Southern California. Soc. Econ. Geol. Guidebook Ser*, *12*, 4-15.

Simon, D. E., & Anderson, M. S. (1990). Stability of clay minerals in acid. *SPE Formation Damage Control Symposium*. Society of Petroleum Engineers. https://doi.org/10.2118/19422-MS

Sirbescu, M. L. C., Krukowski, E. G., Schmidt, C., Thomas, R., Samson, I. M., & Bodnar, R. J. (2013). Analysis of boron in fluid inclusions by microthermometry, laser ablation ICP-MS, and Raman spectroscopy: Application to the Cryo-Genie Pegmatite, San Diego County, California, USA. *Chemical Geology*, *342*, 138-150. https://doi.org/10.1016/j.chemgeo.2013.01.014

Smith, G. L., Almond, H., & Sawyer, D. L. (1958). Sassolite from the Kramer borate district, California. *American Mineralogist: Journal of Earth and Planetary Materials*, *43*(11-12), 1068-1078.
Smith, G. I., & Stuiver, M. (1979). *Subsurface stratigraphy and geochemistry of late Quaternary evaporites, Searles Lake, California*, US Geological Survey, Professional Paper, 1043, 130.

Stack, K. M., Grotzinger, J. P., Lamb, M. P., Gupta, S., Rubin, D. M., Kah, L. C., et al. (2018). Evidence for plunging river plume deposits in the Pahrump Hills member of the Murray formation, Gale crater, Mars. *Sedimentology*. https://doi.org/10.1111/sed.12558

Stanley, C. J., Jones, G. C., Rumsey, M. S., Blake, C., Roberts, A. C., Stirling, J. A., et al. (2007). Jadarite, $LiNaSiB_3O_7$ (OH), a new mineral species from the Jadar Basin, Serbia. *European Journal of Mineralogy 19(4)*, 575-580. https://doi.org/10.1127/0935-1221/2007/0019-1741

Starkey, H. C. (1982). *The role of clays in fixing lithium* (No. 1278). US Government Printing Office. https://doi.org/10.3133/b1278F

Stein, N., Grotzinger, J. P., Schieber, J., Mangold, N., Hallet, B., Newsom, H., et al. (2018). Desiccation cracks provide evidence of lake drying on Mars, Sutton Island member, Murray formation, Gale Crater. *Geology*, *46*(6), 515-518. https://doi.org/10.1130/G40005.1

Steinmetz, R. L. (2017). Lithium-and boron-bearing brines in the Central Andes: exploring hydrofacies on the eastern Puna plateau between 23 and 23 30′ S. *Mineralium Deposita*, *52*(1), 35-50. https://doi.org/10.1007/s00126-016-0656-x

Stephenson, J. D., Hallis, L. J., Nagashima, K., & Freeland, S. J. (2013). Boron enrichment in martian clay. *PloS One*, *8*(6), e64624. https://doi.org/10.1371/journal.pone.0064624

Stubican, V., & Roy, R. (1962). Boron substitution in synthetic micas and clays. *American Mineralogist: Journal of Earth and Planetary Materials*, *47*(9-10), 1166-1173.

Sun, V. Z., Stack, K. M., Kah, L. C., Thompson, L., Fischer, W., Williams, A. J., et al. (2019). Late-stage diagenetic concretions in the Murray formation, Gale crater, Mars. *Icarus*, *321*, 866-890. https://doi.org/10.1016/j.icarus.2018.12.030

Sun, V. Z., Stack, K. M., Nachon, M., Johnson, S. S., Kronyak, R. E., Wiens, R. C., et al. (2018). *Late-Stage Diagenesis in the Murray Formation, Gale Crater, Mars: Evidence from Diverse Concretion Morphologies*. Abstract number 1587. Presented at the 49th Lunar and Planetary Science Conference, Houston, TX.

Tanner, L. H. (2002). Borate formation in a perennial lacustrine setting: Miocene–Pliocene furnace creek formation, Death Valley, California, USA. *Sedimentary Geology*, *148*(1-2), 259-273. https://doi.org/10.1016/S0037-0738(01)00221-4

Thomas, N. H., Ehlmann, B. L., Meslin, P. Y., Rapin, W., Anderson, D. E., Rivera-Hernández, F., et al. (2019). Mars Science Laboratory Observations of Chloride Salts in Gale Crater, Mars. *Geophysical Research Letters*. https://doi.org/10.1029/2019GL082764

Thomas, N. H., Ehlmann, B. L., Meslin, P. Y., Cousin, A., Forni, O., Rapin, W., et al. (2018). *MSL ChemCam Observations of Chloride Salts in Gale Crater, Mars.* Abstract number 2876. Presented at the 49th Lunar and Planetary Science Conference.

Thompson, L. M., Fraeman, A. A., Berger, J. A., Rampe, E. B., Boyd, N. I., Gellert, R., et al. (2019). Compositional Characteristics and Trends Within the Vera Rubin Ridge, Gale Crater, Mars as Determined by APXS: Sedimentary, Diagenetic and Alteration History. Abstract number 3269. Presented at the 50th Lunar and Planetary Science Conference.

Tivey, M. K., Mills, R. A., & Teagle, D. A. (1998). Temperature and salinity of fluid inclusions in anhydrite as indicators of seawater entrainment and heating in the TAG active mound. Presented at the *Proceedings-ocean drilling program scientific results* 158(179-192). National science foundation, Alexandria, VA.

You, C. F., Spivack, A. J., Gieskes, J. M., Martin, J. B., & Davisson, M. L. (1996). Boron contents and isotopic compositions in pore waters: a new approach to determine temperature induced artifacts—geochemical implications. *Marine Geology*, *129*(3-4), 351-361. https://doi.org/10.1016/0025-3227(96)83353-6

Vaniman, D. T., Martínez, G. M., Rampe, E. B., Bristow, T. F., Blake, D. F., Yen, A. S., et al. (2018). Gypsum, bassanite, and anhydrite at Gale crater, Mars. *American Mineralogist: Journal of Earth and Planetary Materials*, *103*(7), 1011-1020. https://doi.org/10.2138/am-2018-6346

Vaniman, D. T., Bish, D. L., Ming, D. W., Bristow, T. F., Morris, R. V., Blake, D. F., et al. (2014). Mineralogy of a mudstone at Yellowknife Bay, Gale crater, Mars. *Science*, *343*(6169), 1243480. https://doi.org/10.1126/science.1243480

Vasavada, A. R., Grotzinger, J. P., Arvidson, R. E., Calef, F. J., Crisp, J. A., Gupta, S., et al. (2014). Overview of the Mars Science Laboratory mission: Bradbury landing to Yellowknife Bay and beyond. *Journal of Geophysical Research: Planets*, *119*(6), 1134-1161. https://doi.org/10.1002/2014JE004622

Vine, J. D., & Dooley J. R. (1980). *Where on Earth is all the lithium? with a section on uranium isotope studies*. No. 80-1234. US Geological Survey. Open-File Report. Series number 80-1234. https://doi.org/10.3133/ofr801234

Wiens, R. C., Maurice, S., Barraclough, B., Saccoccio, M., Barkley, W. C., Bell, J. F., et al. (2012). The ChemCam instrument suite on the Mars Science Laboratory (MSL) rover: Body unit and combined system tests. *Space Science reviews*, *170*(1-4), 167-227. https://doi.org/10.1007/s11214-012-9902-4

Wiens, R. C., Maurice, S., Lasue, J., Forni, O., Anderson, R. B., Clegg, S., et al. (2013). Pre-flight calibration and initial data processing for the ChemCam laser-induced breakdown spectroscopy instrument on the Mars Science Laboratory rover. *Spectrochimica Acta Part B: Atomic Spectroscopy*, *82*, 1-27. https://doi.org/10.1016/j.sab.2013.02.003

Wiens, R. C., Maurice, S., & MSL Science Team. (2015). ChemCam: Chemostratigraphy by the first Mars microprobe. *Elements*, *11*(1), 33-38. https://doi.org/10.2113/gselements.11.1.33

Williams, L. B., Hervig, R. L., Holloway, J. R., & Hutcheon, I. (2001). Boron isotope geochemistry during diagenesis. Part I. Experimental determination of fractionation during illitization of smectite. *Geochimica et Cosmochimica Acta*, *65*(11), 1769-1782. https://doi.org/10.1016/S0016-7037(01)00557-9

Williams, A. E., & Taylor, M. C. (1996). Mass spectrometric identification of boric acid in fluid inclusions in pegmatite minerals. *Geochimica et Cosmochimica Acta*, *60*(18), 3435-3443. https://doi.org/10.1016/0016-7037%2896%2900151-2

You, C. F., Spivack, A. J., Gieskes, J. M., Martin, J. B., & Davisson, M. L. (1996). Boron contents and isotopic compositions in pore waters: a new approach to determine temperature induced artifacts—geochemical implications. *Marine Geology*, *129*(3-4), 351-361. https://doi.org/10.1016/0025-3227(96)83353-6

Zhao, J., Lin, W., Chang, Q., Li, W., and Lai, Y. (2012). Adsorptive characteristics of akaganeite and its environmental applications: a review. *Environmental Technology Reviews*, *1*(1), 114-126, http://dx.doi.org/10.1080.09593330.2012.701239.

Zolensky, M. E. (2010). Liquid water in asteroids: Evidence from fluid inclusions in meteorites. In *Astrobiology Science Conference 2010: Evolution and Life: Surviving Catastrophes and Extremes on Earth and Beyond* (Vol. 1538, p. 5278).

Zolensky, M. E., Bodnar, R. J., Gibson, E. K., Nyquist, L. E., Reese, Y., Shih, C. Y., & Wiesmann, H. (1999). Asteroidal water within fluid inclusion-bearing halite in an H5 chondrite, Monahans (1998). *Science*, *285*(5432), 1377-1379. http://doi.org/10.1126/science.285.5432.1377